International Journal of Fatigue 182 (2024) 108200

Contents lists available at ScienceDirect

International Journal of Fatigue

journal homepage: www.elsevier.com/locate/ijfatigue

Fatigue experiment and assessment of butt-welded joints in steel structures considering misalignment and weld geometry effects

Pengjun Luo [a,*], Yuta Mashino [b], Yuki Matsuo [b], Yuki Kasaoka [b], Seiichiro Tsutsumi [a,*]

[a] Graduate School of Engineering, Osaka University, Osaka 565-0871, Japan
[b] Komatsu Manufacturing Co., Ltd., Hirakata 573-1011, Japan

ARTICLE INFO

Keywords:
Butt-welded joint
Fatigue
Misalignment
Weld geometry
Stress concentration

ABSTRACT

This study investigates the fatigue behavior of butt-welded joints considering the effects of misalignments and weld geometries. Fourteen specimens were fabricated with varied assembly root gaps and axial eccentricities, and they were subjected to cyclic tensile loading with constant amplitude. Misalignments (both axial and angular) and weld geometries (including weld toe radius, flank angle, weld reinforcement height, and width) were measured using a 3D optical scanning system and subsequently used for fatigue evaluation in terms of fatigue crack locations and fatigue strength. The fatigue test results indicate a noticeable decrease in nominal stress fatigue strength as the assembled axial eccentricities increase, regardless of the assembled root gaps. However, the correlation between assembled root gaps and fatigue strength is not clear, as a larger assembled root gap corresponds to a flatter weld reinforcement on one hand and an increase in angular misalignment on the other hand. Several stress magnification factor (SMF) and stress concentration factor (SCF) formulae available in the literature are employed to characterize the combined effects of misalignment and weld geometries. The investigation results indicate that misalignments and weld geometries both play critical roles in the fatigue behavior of butt-welded joints. The combination of Remes and Varsta's SCF formula with Luo et al.'s SMF formula is the most recommended method due to its accuracy and robustness regarding the evaluation of both the fatigue crack locations and fatigue life in the investigated butt-welded joints.

1. Introduction

Owing to its characteristics of simplicity, versatility, and cost-effectiveness, the butt-welded joint is widely utilized in civil and industrial structures, encompassing applications in buildings, bridges, ships, offshore installations, and so on [1–4]. However, the inherent features of the welding process often result in welded joints exhibiting reduced fatigue strength compared to the steel plates they connect. Consequently, these welded joints are often the most vulnerable sites for the initiation of fatigue cracks when the welded structures are subjected to cyclic loadings. Evaluating the fatigue properties of welded joints can be a complex, expensive, and time-consuming task. This complexity arises from the interaction of numerous factors, including the welding process-induced deformations and residual stresses [5], the weld defects and geometries [6], the loading conditions [7], and the environmental factors [8]. So far, extensive research has been conducted to understand the fatigue behavior of butt-welded joints, with a particular focus on the influences induced by the misalignments and weld geometries.

A certain degree of misalignment, both axial and angular, is typically inevitable in butt-welded joints, even when great care is taken during the fabrication process. Braun and Kellner [9] conducted a comprehensive investigation using machine learning techniques to identify influential features and their interactions affecting fatigue failure locations and fatigue strength in 621 fatigue test data of butt-welded joints. Their findings revealed that axial and angular misalignments emerged as the primary parameters for classifying failure locations and also played a significant role as the secondary factor in predicting fatigue life. The presence of the misalignments would result in the stress increasing in a welded joint, primarily due to the occurrence of secondary bending when the joint is subjected to an axial load [10,11]. As a result, the nominal stress-characterized fatigue strength of the butt-welded joints significantly decreases as axial and angular misalignments increase [12,13]. When applying the fatigue assessment approach recommended in standards and design guidelines[14,15], while a certain degree of misalignment influence is considered through the corresponding FAT class S-N curves, it becomes necessary to factor in the secondary bending

* Corresponding authors.
E-mail addresses: luo@civil.eng.osaka-u.ac.jp (P. Luo), tsutsumi@civil.eng.osaka-u.ac.jp (S. Tsutsumi).

https://doi.org/10.1016/j.ijfatigue.2024.108200
Received 31 October 2023; Received in revised form 16 January 2024; Accepted 5 February 2024
Available online 8 February 2024

stress induced by axial or angular misalignment if the misalignment exceeds the specified permissible level. This is typically accomplished by multiplying the applied stress by an additional stress magnification factor (SMF) [14,16,17], which is always greater than or equal to 1.0. By doing so, the scatter of the fatigue test data is reduced, and the accuracy of fatigue strength prediction is indeed improved to some degree under the nominal stress evaluation system [12,16,18]. However, SMF formulae specified in IIW recommendations are no longer accurate and consistently conservative when employing local stress methods for fatigue evaluation [19]. As clearly indicated by the test results of [18,20], the fatigue cracks might originate at any of the four weld toes (or weld root). This implies that, when superimposing the misalignment induced secondary bending stress, the local stress at the potential fatigue crack sites can either increase or decrease, rather than always increaseing. Because of the fact that the secondary bending stress induced by the straightening of the specimen under axial loading would be either positive or negative, depending on the concave and convex sides [19,21]. The conventional SMF formulae are no longer effective when considering the varying effects of misalignment on different weld toes (or weld roots), posing a challenge in predicting the fatigue crack initiation sites.

Extensive investigations have clearly shown that the weld geometries are directly related to the fatigue life of weld joints [22–27]. For a butt-welded joint experiencing fatigue failure at the weld toe, the most representative and critical weld geometry parameters include the weld toe radius, weld flank angles, weld reinforcement height, weld reinforcement width, and undercut. One of the most widely used approaches to consider the weld geometry effect on the fatigue behavior of butt-welded joints is through the use of the stress concentration factor (SCF), which is defined as the ratio of local stress to nominal stress [27–31]. Teng et al. [32] reported that decreasing the flank angle is more effective than increasing the weld toe radius in improving the fatigue crack initiation life of butt-welded joints. However, Gao et al. [33] emphasized the more pronounced effect of weld toe radius compared to the flank angle on the fatigue reliability index of butt-welded joints. According to Remes and Varsta [27], for laser-welded joints with significantly smaller weld bead sizes compared to arc-welded joints, the dominant geometrical parameters affecting local stresses are weld reinforcement height, weld reinforcement width, and notch depth, while the flank angle has a minor influence. Cerit et al. [34] reported that in undercut-free butt-welded joints, larger flank angles and smaller weld toe radii result in higher SCF values. In the case of butt-welded joints with undercuts, the severity of SCF is primarily governed by the ratio of depth to radius of the undercut and the width of the undercut. Niraula et al. [35] observed that the primary fatigue cracks tended to initiate at the deepest notches rather than at the sharpest radii, highlighting the undercut depth as the most influential parameter in primary fatigue crack initiation for the butt-welded joints containing undercut defects. Bell et al. [36] found that undercuts deeper than 0.5 mm significantly reduced fatigue life, while those under 0.25 mm had a negligible effect on an arc-welded T-joint. In the fracture mechanics-based studies, Wang et al. [37] reported that the stress intensity factor (SIF) of a center-cracked butt-welded joint under tensile loading decreases with an increase in weld reinforcement height and width, while the influence of the weld toe radius can be disregarded. Laguna et al. [38] also indicated that weld reinforcement height has a more significant influence on the fatigue life of shielded metal arc welding (SMAW) butt joints compared to the weld toe radius. Furthermore, the investigation conducted by Schork et al. [39] revealed that the most influential parameter for the fatigue life of butt-welded joints was the undercut, followed by weld flank angle and weld toe radius. Most recently, Braun and Kellner [9] conducted an investigation using machine learning techniques. Their findings revealed that, among the previously mentioned weld geometrical parameters, the depth of undercut exhibited the strongest correlation to the fatigue crack location, followed by weld toe radius and weld reinforcement height. As for fatigue life, the strongest correlating factor was weld reinforcement height, followed by weld reinforcement width and weld toe radius.

Previous studies mentioned above present conflicting conclusions regarding the effect of weld geometries on the fatigue properties of butt-welded joints. Some works suggest that the dominant influential factors are the weld reinforcement height and width, with the influence of weld toe radius and/or weld flank angle considered negligible [9,27,37,38]. Conversely, other studies have stated that the influences of weld toe radius and weld flank angle are also significant, potentially even serving as dominant factors [32–34,39]. In addition, the investigation on the combined effects of misalignment and weld geometries is limited. In the current study, fourteen butt-welded joints are fabricated with varied assembly root gaps and axial eccentricities and tested under constant amplitude load condition. An optical 3D scanning system is employed to acquire the 3D spatial point cloud data for the profile of each specimen, based on which the misalignments (including both axial and angular) and weld geometries (including weld toe radius, flank angle, weld reinforcement height and width) are determined through the multi-sectional shape analysis. The obtained misalignments and weld geometries are then utilized to estimate the fatigue crack location and fatigue strength of the tested butt-welded joints, based on several existing SMF and SCF formulas that are well-documented in the literature. Based on the investigation results, the combined effects of misalignment and weld geometries are effectively characterized, and formulae that perform well in predicting both fatigue crack location and fatigue strength are proposed.

2. Fatigue experiments

2.1. Specimen preparation

In this study, a total of fourteen butt-welded joint specimens were fabricated and tested. Fig. 1 illustrates the schematic configurations for the preparation of butt-welded joint specimens. Two SS400 steel plates, with nominal dimensions of 400 mm × 150 mm × 16 mm, were initially preprocessed with a bevel angle of 35° and a zero-root face depth for edge preparation. Subsequently, they were temporarily assembled using three 40 mm long track welds, spaced at intervals of 140 mm. The assembling root gap (*RG*) was varied between 0 mm, 1 mm, and 2 mm, while three different assembling axial eccentricities (e_a) of 0 mm, 1 mm, and 3 mm were introduced between the two steel plates to be joined. To achieve the one-side full penetration butt welds, four layers were deposited in a flat position, utilizing the CO2 gas-shielded metal arc welding (GMAW) process with the JIS Z3312 YGW18 electrode. Two dog-bone-shaped specimens with identical assembly parameters were obtained by extracting from the middle part between the two tack welds of the butt-welded joint prototypes.

2.2. Weld geometry measurement

2.2.1. Measurement procedure

Before conducting fatigue tests, geometry measurements were taken on each specimen using a commercial optical measurement system, specifically the Keyence VL360 as shown in Fig. 2(a), which offers a measurement accuracy of ± 10 μm with a measurement range of 300 mm × 200 mm. The butt-welded joints were cleaned and either powder-coated (for specimens 1 to 6) or lacquer-sprayed (for specimens 7 to 14) before scanning. This process was carried out to enhance reflectivity and eliminate any excessively shining points on the surface. Then, 3D scanning was conducted to acquire point cloud data of the specimen's surface, seeing Fig. 2(b) as an example. Subsequently, the point cloud data in 3D space was transformed into individual 2D sections by slicing along a single plane perpendicular to the welding length direction. Fig. 2 (c) shows an example of the 2D sectional profiles generated from the 3D-scanned specimen using the splitting planes. Splitting was made with an interval of 0.1 mm. The data within a distance of approximately 0.5 mm near the ends of the weld was excluded from the data analysis, which

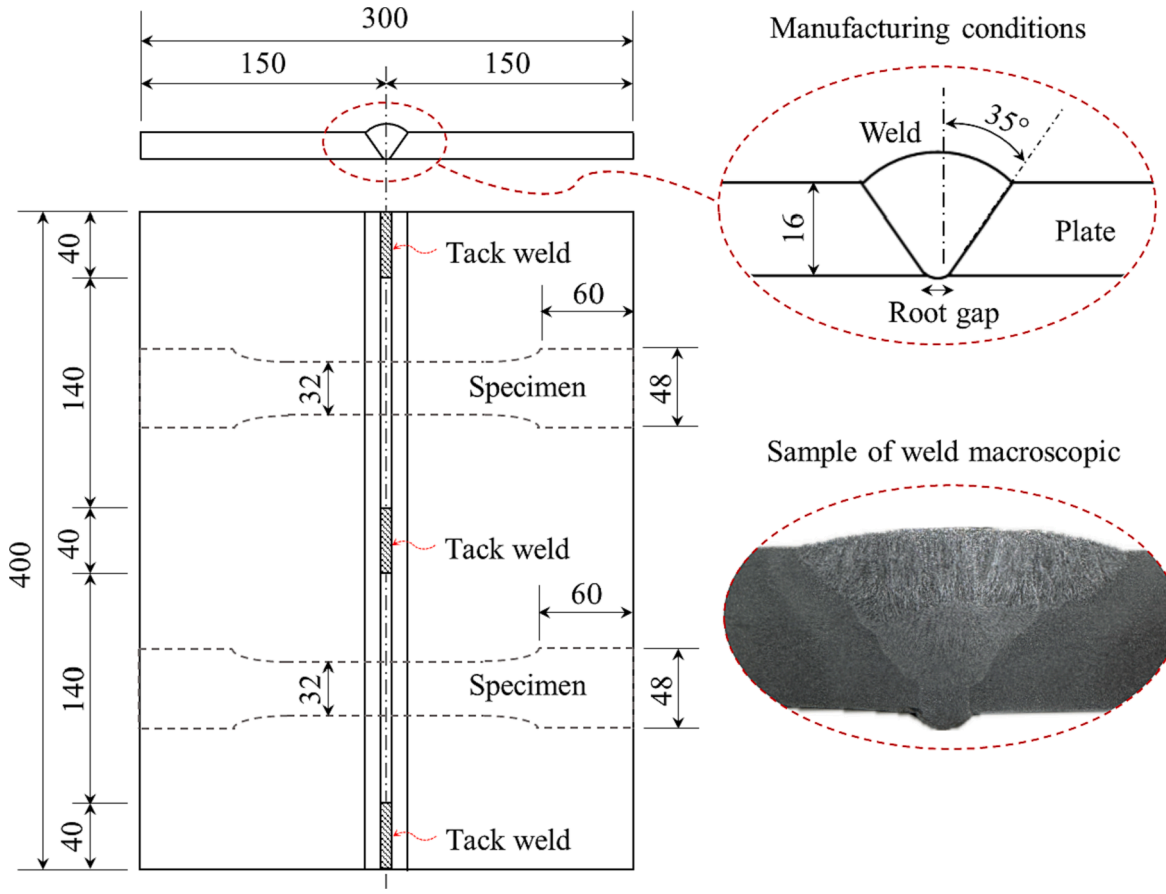

Fig. 1. Schematic for the preparation of the butt-welded joint specimens (units in millimeters).

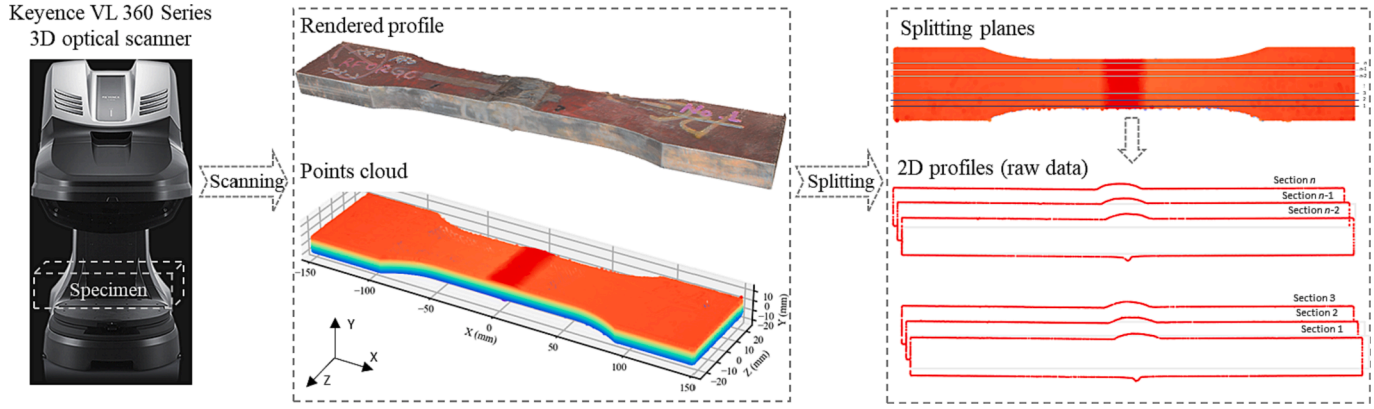

Fig. 2. Illustration of weld geometry measurement flowchart.

was necessary to mitigate potential data deviations caused by the lower accuracy of 3D scanning for the specimen edges. Therefore, a total of 311 cuts were made for each specimen currently investigated, and the resulting 2D data sets would serve as the foundational database for determining both the misalignments and the weld geometries.

As illustrated in Fig. 3, the axial misalignment (e) is quantified as the eccentricity between two steel plates at the weld center, whereas the angular misalignment (α) is assessed by measuring the acute angle formed between the two steel plates. By utilizing data points outside the weld area of each 2D sectional database, two straight lines representing the surfaces of the left and right steel plates are obtained by curve fitting. Subsequently, the offset value between these two straight lines at the weld center position as well as the acute angle between them are computed. The average of the offset values, both for the front and back sides, was taken as the axial misalignment, while the average of the acute angles represented the angular misalignment. The measured axial misalignments range from −0.45 mm to 2.09 mm and generally increase as the assembling axial eccentricities increase. Despite taking extreme care to avoid any angular misalignments during assembly, the influence of welding residual deformation still resulted in varying degrees of angular misalignment observed in all specimens, ranging from 0.46° to 2.98°.

The measurements of weld geometry include the weld reinforcement height (h), weld reinforcement width (w), weld toe radius (r), and weld flank angle (θ), with their definitions shown in Fig. 3. The weld reinforcement width (w) is calculated as the distance between two weld toes.

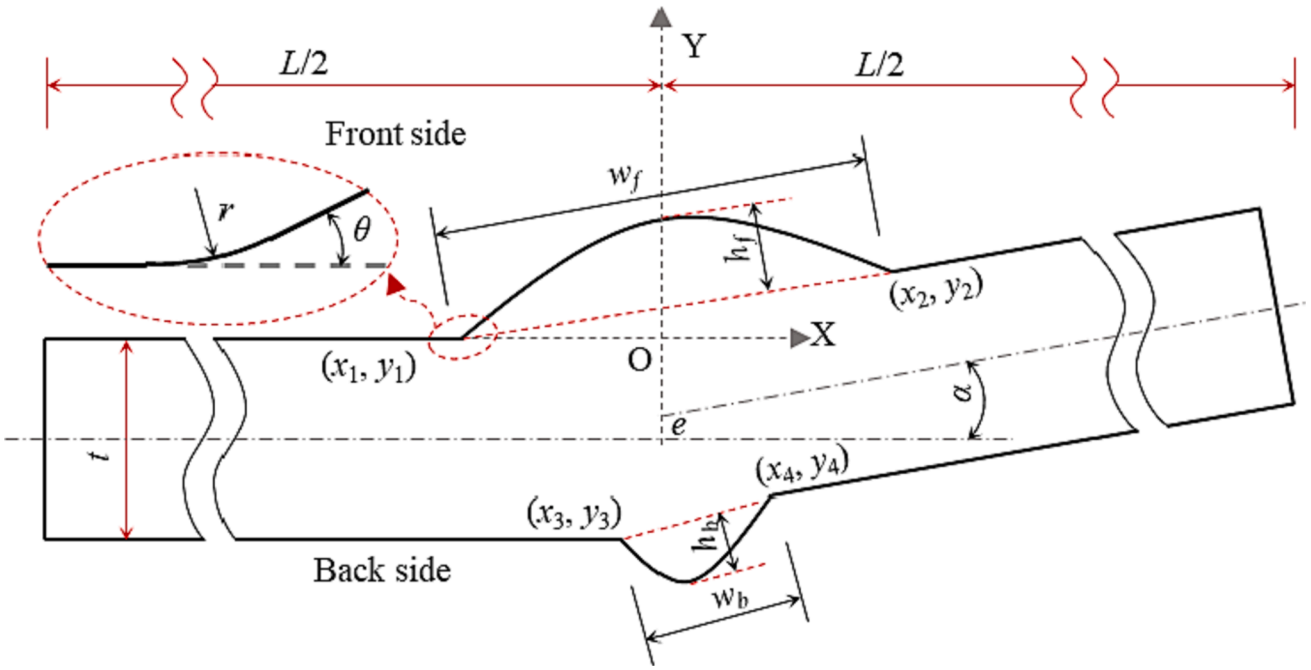

Fig. 3. Definition of weld geometrical parameters for a butt-welded joint.

For the front side reinforcement, it is measured as the distance between points (x_1, y_1) and (x_2, y_2), while for the back-side reinforcement, it is measured as the distance between points (x_3, y_3) and (x_4, y_4). The weld reinforcement height (h) is determined as the maximum distance from the point on the weld reinforcement to the straight line formed by the corresponding two weld toes. The local geometries included the weld toe

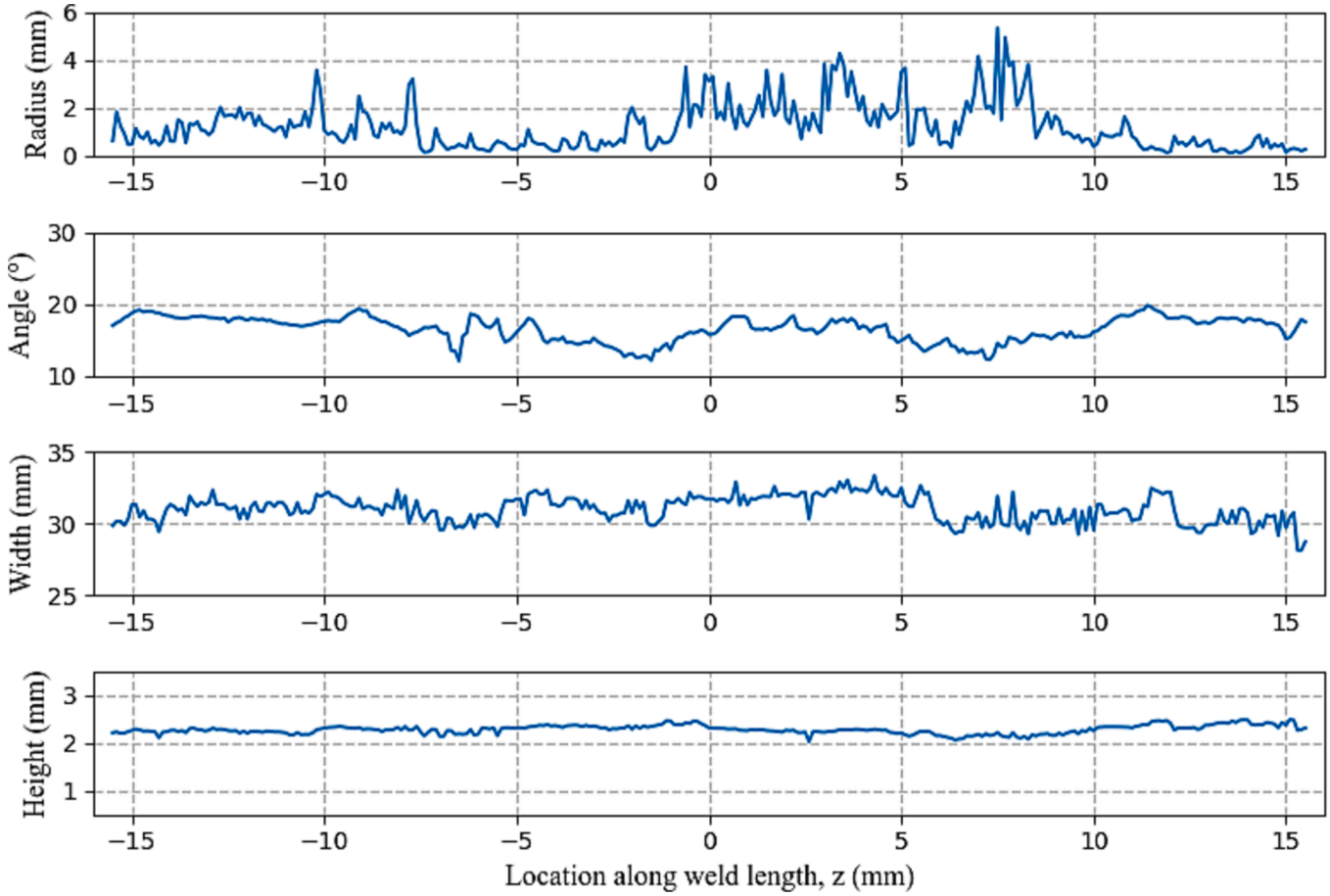

Fig. 4. Example of weld geometry measurement results along the weld length.

radius (r) and weld flank angle (θ). The weld toe radius is determined using the curvature method, as recommended in [40]. The location of the weld toe is determined as the point where the maximum curvature along the x-coordinate occurs, and the weld toe radius is calculated as the reciprocal value of the corresponding curvature at this location. The weld flank angle is measured as the acute angle between the steel plate surface and the weld bead surface.

2.2.2. Geometry measurement results

Fig. 4 presents an example of weld geometry measurement results taken along the weld length with an interval of 0.1 mm. It is noteworthy that due to both the inherent non-stationarity of the welding process and the potential measurement inaccuracies, all the weld geometrical parameters exhibit significant variations along the length of the weld seam. As one-side full penetration V-type butt-welded joints may experience fatigue failure from both sides, weld geometrical parameters of both the weld front side and weld back side are measured for all specimens. The measured results, including average value (denoted as Avg.) and standard deviations (denoted as Std.), are summarized in Table 1 for the weld front side and in Table 2 for the weld back side. It is important to mention that the outliers have been removed from the database for statistical analysis by using the Inter Quartile Range (IQR) method [41] with a threshold factor of 1.5. As shown in Table 1 and Table 2, the reinforcement heights are comparable for both the weld front and back sides. However, the reinforcement widths are over 30 mm for the weld front side but below 10 mm for the weld back side, indicating the formation of a smaller but steeper weld profile on the back side. Additionally, the average values of weld toe radius and flank angle exhibit significant variations between specimens, as well as between the left and right weld toes, and also between the weld front side and weld back side. However, it is observed that, on average, the powder-coated specimens (1 to 6) have smaller weld toe radii compared to the lacquer-sprayed specimens (7 to 14). These variations might be the contributing factors to the significant differences in fatigue crack locations and fatigue life of each specimen.

Fig. 5 shows the Pearson Correlation Coefficient matrix between the investigated weld geometrical parameters and the two assembling parameters (i.e., RG and e_a). It is worth noting that measured axial misalignment (e) is used instead of the assembling one (e_a) due to their strong positive correlation. The measured axial misalignment (e) and angular misalignment (α) are detailed in Table 3 in the subsequent Section 2.3. Additionally, r_f and r_b in the plot denote the average radii of the left and right weld toes for the weld front and back sides, respectively; while θ_f and θ_b represent the average flank angle of the left and right weld toes for the weld front and back sides. The results indicate a strong negative correlation between the assembling root gap (RG) and the ratio of weld reinforcement height to width (i.e., h_f / w_f and h_b / w_b), with correlation coefficients of −0.883 and −0.877 for the weld front side and back side, respectively. This suggests that a larger assembling root gap would result in a flatter weld reinforcement. The possible reason is that the larger assembling root gap resulted in a broader weld pool, making the filler material more prone to flow during the welding process. Additionally, the angular misalignment (α) demonstrates a positive correlation with the axial misalignment (e), supported by a correlation coefficient of 0.719. Furthermore, it is noteworthy that the weld flank angle and the weld toe radius exhibit a relatively strong negative correlation, with correlation coefficients of −0.841 for the weld front side (between θ_f and r_f) and −0.853 for the weld back side (between θ_b and r_b), respectively.

2.3. Test conditions and results

Fatigue tests were conducted using a Servo Hydraulic Fatigue Testing Machine with a maximum load capacity of 300 kN. The specimens were subjected to axially tensile loading cycles with a constant amplitude scenario. Across different specimens, the minimum load (P_{min}) was consistently maintained at 5 kN, while the maximum load (P_{max}) varied in the range of 100 kN to 120 kN. Consequently, the corresponding nominal stress range ($\Delta\sigma$) fell between 186 MPa and 225 MPa. Due to the presence of angular misalignment, all specimens have a convex back side and a concave front side. When a specimen is mounted and held by the grip fixtures, the angular misalignment is partially straightened. As a result, tensile stress is induced on the front side, while compression stress is experienced on the back side, with the magnitudes depending on the degree of angular misalignment. The tests were terminated either when the specimen fractured completely or when the number of loading cycles reached 4 million. With the exception of specimen 6, all the other specimens fractured before reaching 4 million loading cycles. Additionally, despite the smaller weld toe radius and larger flank angle on the weld back side for several specimens, as indicated in Table 1 and Table 2, fatigue cracks are observed to originate at the weld front side rather than the weld back side for all specimens. The test conditions and results are summarized in Table 3. To facilitate the comparison of fatigue strength among specimens that underwent cyclic loadings with varying load ranges, an equivalent fatigue strength corresponding to 2 million loading cycles ($\Delta\sigma_{eq}$) has also been calculated using Eq. (1) and is included in Table 3.

$$\Delta\sigma_{eq} = \left[N_f / \left(2 \times 10^6\right)\right]^{1/m} \bullet \Delta\sigma \tag{1}$$

where N_f represents the number of loading cycles until the specimen fractures, also referred to as total fatigue life, and m is set to 3 in accordance with the IIW Recommendation [14].

Table 1
Summary of geometrical results for weld front side.

ID	Height, h_f (mm)		Width, w_f (mm)		Radius, r (mm)				Flank angle, θ (°)			
	Avg.	Std.	Avg.	Std.	Left toe		Right toe		Left toe		Right toe	
					Avg.	Std.	Avg.	Std.	Avg.	Std.	Avg.	Std.
1	2.27	0.08	30.98	0.88	1.06	0.74	2.47	2.10	16.58	1.71	11.72	1.10
2	2.22	0.12	31.06	0.95	0.90	0.60	0.75	0.59	17.61	2.08	16.56	1.62
3	2.29	0.08	34.31	1.06	1.01	0.82	1.00	0.76	15.54	1.75	16.25	1.81
4	2.30	0.11	35.02	0.98	1.21	0.83	0.73	0.45	12.61	2.12	18.58	1.33
5	1.70	0.09	34.93	0.99	0.69	0.42	0.87	0.77	18.24	2.51	12.07	2.13
6	1.70	0.09	35.56	0.86	0.77	0.62	1.74	1.08	13.79	1.69	13.61	1.33
7	1.82	0.08	32.07	0.43	1.93	0.73	3.07	1.23	14.79	1.67	5.58	1.61
8	2.10	0.05	31.75	0.60	1.60	0.61	2.23	1.11	17.22	1.49	11.39	1.63
9	2.18	0.08	32.30	0.61	1.26	0.46	2.27	1.09	22.33	2.37	6.63	1.98
10	2.25	0.07	32.01	0.67	0.98	0.39	1.92	0.90	22.24	1.94	9.82	1.19
11	1.77	0.06	32.74	0.53	2.03	0.76	2.68	1.06	14.18	1.52	5.19	1.04
12	1.45	0.09	32.22	0.98	2.20	0.94	2.44	1.23	11.50	1.70	4.28	1.78
13	1.75	0.09	30.77	1.76	1.50	0.54	2.63	1.16	17.33	2.08	1.35	0.71
14	1.70	0.10	31.30	1.99	1.35	0.48	2.31	1.07	18.02	1.76	2.58	1.34

Table 2
Summary of geometrical results for weld back side.

ID	Height, h_b (mm)		Width, w_b (mm)		Radius, r (mm)				Flank angle, β (°)			
	Avg.	Std.	Avg.	Std.	Left toe		Right toe		Left toe		Right toe	
					Avg.	Std.	Avg.	Std.	Avg.	Std.	Avg.	Std.
1	1.24	0.14	5.43	0.83	0.79	0.41	0.49	0.30	22.58	6.82	31.00	10.27
2	1.40	0.14	5.38	0.62	0.39	0.20	0.37	0.18	28.29	6.98	40.46	3.93
3	1.49	0.11	6.94	0.67	0.73	0.27	0.71	0.38	31.87	3.86	28.42	7.82
4	1.60	0.11	7.39	0.61	0.64	0.33	0.30	0.15	29.68	6.87	31.41	5.50
5	1.58	0.11	7.73	0.53	0.83	0.36	0.65	0.31	29.16	4.61	34.21	3.40
6	1.59	0.10	8.24	0.69	0.81	0.32	0.33	0.17	31.84	4.33	28.28	6.34
7	1.65	0.10	7.89	0.50	1.83	0.54	0.88	0.30	22.10	4.02	37.72	1.96
8	1.42	0.12	6.57	0.79	0.77	0.33	0.67	0.24	22.10	6.76	36.50	4.93
9	1.61	0.11	7.87	0.56	1.83	0.78	0.63	0.19	13.38	3.94	43.54	1.33
10	1.38	0.11	6.18	0.53	1.93	0.48	0.67	0.18	14.39	2.26	46.26	1.46
11	1.60	0.17	9.01	0.55	1.68	0.72	0.56	0.25	19.78	4.39	33.34	4.62
12	1.60	0.05	8.57	0.44	1.00	0.45	0.80	0.24	22.83	4.73	33.33	1.75
13	1.56	0.09	8.91	0.32	2.67	1.16	0.74	0.17	13.59	3.39	41.84	1.28
14	1.51	0.13	9.50	0.67	8.03	4.78	0.99	0.47	9.97	1.34	28.47	3.90

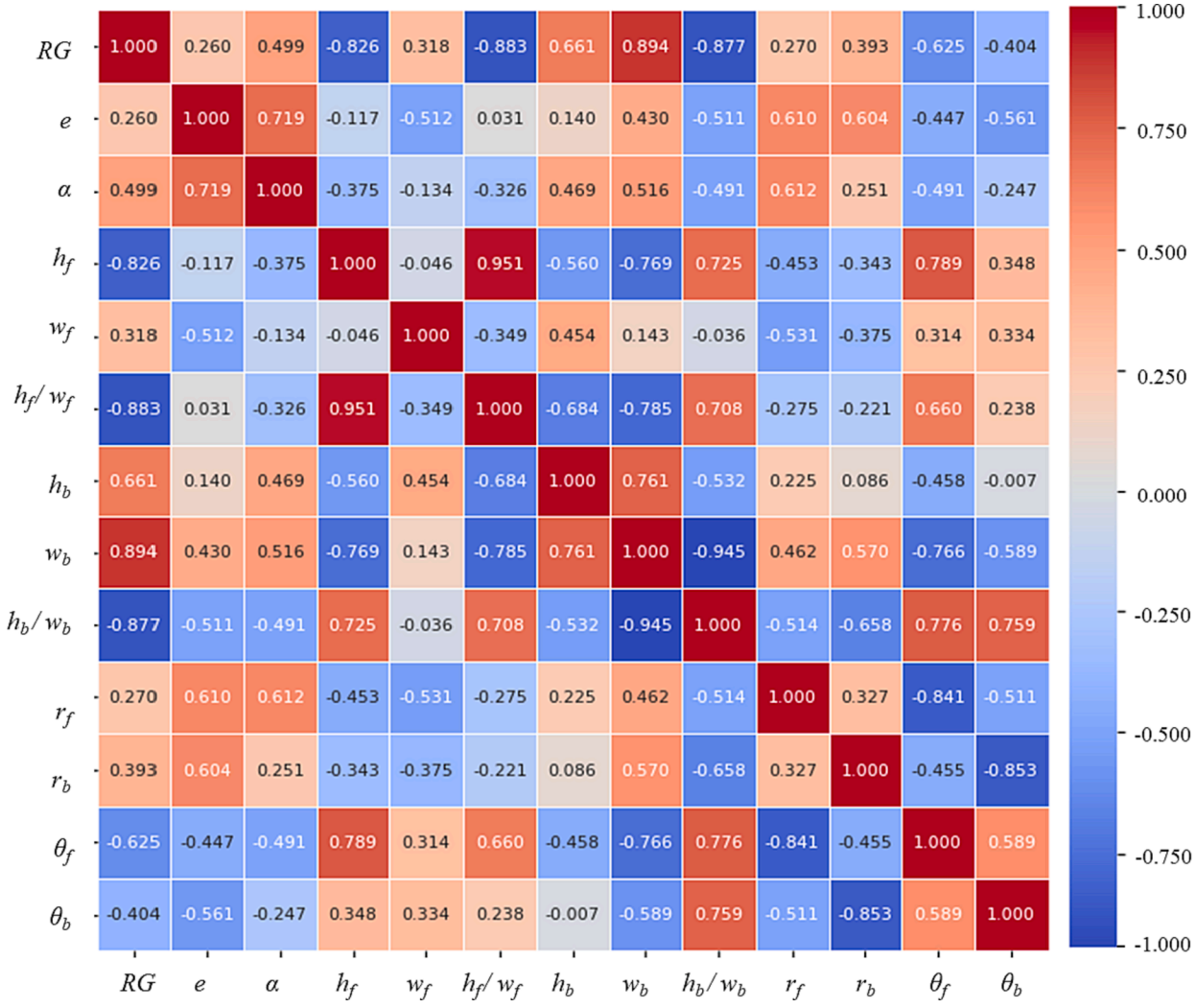

Fig. 5. Pearson Correlation Coefficients matrix for the investigated parameters.

Fig. 6 illustrates the effects of the assembled root gap on the equivalent fatigue strength with different assembled axial misalignment conditions. For specimens with zero assembled axial misalignment (see Fig. 6(a)), the average fatigue strength slightly decreases from 151.9 MPa to 141.5 MPa with an increase in the assembled root gap from 0 mm to 1 mm. This decline may be attributed to the difference in angular misalignment, as indicated in Table 3, with average values of 0.52° for specimens with $RG = 0$ mm and 1.13° for those with $RG = 1$ mm, respectively. Notably, when the assembled root gap increases to 2 mm, the average fatigue strength significantly rises to about 214.7 MPa,

Table 3
Fatigue loading conditions and test results. (* Fatigue crack location, FL denotes left weld toe of front side, FR denotes right weld toe of front side.)

ID	Assemble parameter		Load condition			Misalignments		Fatigue results		
	RG (mm)	e_a (mm)	P_{max} (kN)	P_{min} (kN)	$\Delta\sigma$ (MPa)	e (mm)	α (°)	N_f (cycles)	$\Delta\sigma_{eq}$ (MPa)	Crack*
1	0	0	120	5	225	0.34	0.46	755,920	162	FL
2	0	0	120	5	225	−0.45	0.57	499,550	141	FL
3	1	0	120	5	225	−0.11	1.09	549,660	146	FR
4	1	0	110	5	205	0.24	1.16	596,830	137	FR
5	2	0	100	5	186	−0.28	1.47	2,342,450	196	FL
6	2	0	100	5	186	0.01	1.48	4,000,000	234	–
7	1	1	120	5	225	1.05	2.19	324,679	123	FL
8	1	1	120	5	225	0.74	2.02	194,394	103	FL
9	1	3	100	5	186	2.09	2.98	162,525	80	FL
10	1	3	120	5	225	1.84	2.90	80,678	77	FL
11	2	1	100	5	186	1.01	2.85	437,008	112	FL
12	2	1	120	5	225	0.69	2.76	270,665	115	FL
13	2	3	100	5	186	1.95	1.96	352,454	104	FL
14	2	3	120	5	225	1.75	1.83	170,660	99	FL

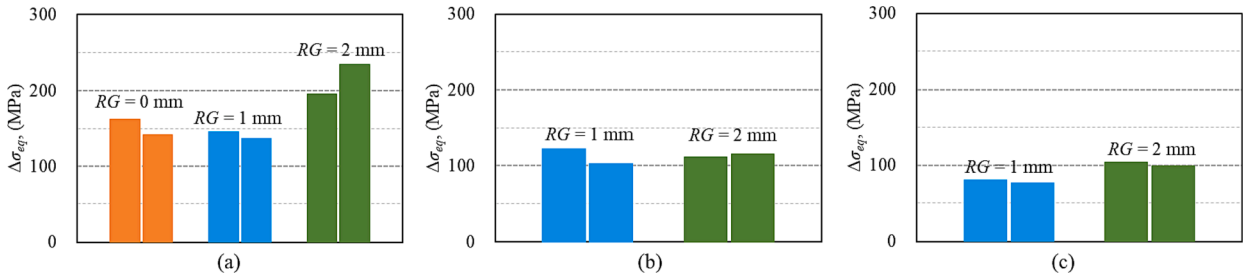

Fig. 6. Effect of assembled root gap on the equivalent fatigue strength: (a) $e_a = 0$ mm; (b) $e_a = 1$ mm; (c) $e_a = 3$ mm.

despite an increase in average angular misalignment to 1.48°. Given that numerous studies have reported a decrease in the weld toe SCF with a reduction in weld reinforcement height [27,29,30], it is rational to attribute the observed increase in fatigue strength to the decrease in weld reinforcement height, from 2.3 mm to 1.7 mm, as indicated in Table 1. For specimens with an assembled axial misalignment of 1 mm (see Fig. 6(b)), no significant difference in fatigue strength was observed when the assembled root gap increased from 1 mm to 2 mm. Conversely, for specimens with an assembled axial misalignment of 3 mm (see Fig. 6 (c)), the fatigue strength increases from about 80 MPa to 100 MPa with the same assembled root gap increment. The rationale becomes clear when examining Table 1 and Table 3, where, in the former case, the angular misalignment increases while the weld reinforcement height decreases, whereas, in the latter case, both the angular misalignment and weld reinforcement height decrease. As previously indicated in Fig. 5, a larger assembling root gap correlates with a flatter weld reinforcement, supported by −0.826 correlation with h_f. Moreover, a 0.499 correlation with α suggests a potential increase in angular misalignment with a larger assembling root gap. The interaction between these two competing factors complicates the evaluation of fatigue properties of butt-welded joints. Fig. 7 illustrates the effects of assembled axial misalignment on the nominal stress fatigue strength with different assembled root gap conditions. As anticipated, primarily due to the secondary bending stress effect, the nominal stress-characterized fatigue strength of butt-welded joints noticeably decreases as the assembled axial misalignments increase, regardless of the assembled root gap.

3. Fatigue evaluation

3.1. Definition of SMF and SCF

Fig. 8 shows a schematic diagram of transversely loaded butt-welded joints under different misalignment conditions. For a butt-welded joint with no misalignment, according to the elementary beam theory, the nominal stress (σ_n) at the weld can be calculated using Eq. (2), in which F represents the applied tensile load, and b and t denote the plate width and thickness of the joint, respectively.

$$\sigma_n = \frac{F}{bt} \tag{2}$$

For a butt-welded joint with either axial or angular misalignment,

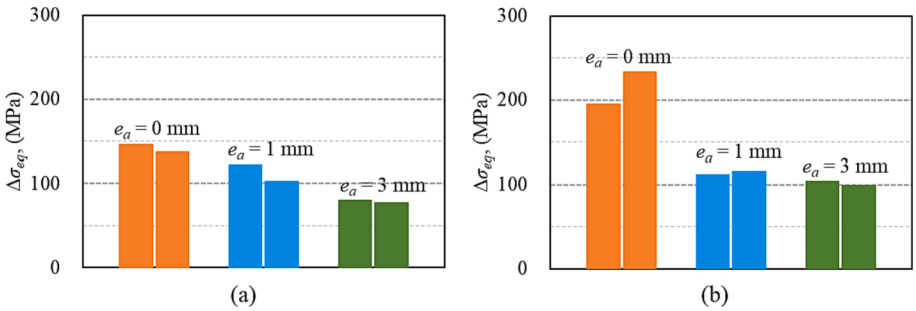

Fig. 7. Effect of assembled axial misalignment on the equivalent fatigue strength: (a) $RG = 1$ mm; (b) $RG = 2$ mm.

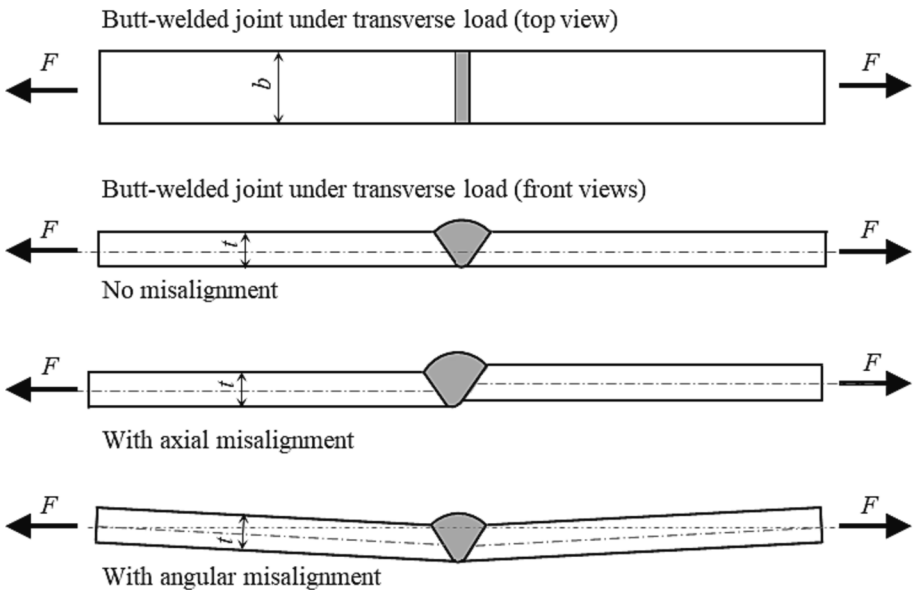

Fig. 8. Illustration of transversely loaded butt-welded joints under various misalignment conditions.

the nominal stress at the weld consists of two parts: one induced directly by the tensile load ($\sigma_{tensile}$), which is the same as that with no misalignment, as indicated by Eq. (2); and the other induced by the secondary bending (σ_{second}), which accounts for the effect of the eccentricity between the tensile load axis and the neutral axis of the joint. The magnitude of secondary bending induced part is proportional to the tensile load and the eccentricity. Therefore, the nominal stress at the weld of a butt-welded joint with misalignment (σ_m) can be calculated using Eq. (3).

$$\sigma_m = \sigma_{tensile} + \sigma_{second} = \left(1 + \frac{\sigma_{second}}{\sigma_{tensile}}\right)\sigma_{tensile} = K_m \bullet \sigma_n \tag{3}$$

where K_m represents the SMF and is defined as Eq. (4).

$$K_m = 1 + \frac{\sigma_{second}}{\sigma_{tensile}} = 1 + \frac{\sigma_{second}}{\sigma_n} \tag{4}$$

When apply the local stress method to account for the weld geometry effect on the fatigue behavior of a weld joint, the local stress is typically defined as the product of nominal stress and the SCF, as shown in Eq. (5) for the case of a butt-welded joint with no misalignment.

$$\sigma_{local} = K_t \bullet \sigma_n \tag{5}$$

Here, K_t represents the SCF. In the case of a butt-welded joint with misalignment, as per Eq. (3), the nominal stress at the weld becomes σ_m due to the inclusion of secondary bending stress. Therefore, the local stress, as defined in Eq. (5), can be expressed as follows:

$$\sigma_{local} = K_t \bullet \sigma_m = K_t \bullet K_m \bullet \sigma_n \tag{6}$$

3.2. SMF formulae

To account for the impact of misalignments on the fatigue performance of welded joints, the formulae of additional SMF have been provided in the IIW Recommendation [14], as indicated by Eqs. (7) and (8) respectively for axial misalignment (K_{me}) and angular misalignment ($K_{m\alpha}$).

$$K_{\mathrm{me}} = 1 + \lambda_e \bullet \frac{e \bullet L_1}{t \bullet (L_1 + L_2)} \tag{7}$$

$$K_{\mathrm{m\alpha}} = 1 + \lambda_\alpha \bullet 1.5 \bullet \frac{\alpha L_f}{2t} \tag{8}$$

where λ_e and λ_α are parameters that account for the boundary condition effects and are respectively equal to 6 and 1 for conservative consideration, in the case of the fixed boundary condition as indicated in Fig. 9. In which, L_1 and L_2 represent the distances from the edge of the fixed and movable clamping fixtures to the center of butt-welded joint specimen, respectively; and L_f denotes the distance between the fixture edges.

Xing and Dong [16] proposed a comprehensive set of analytical SMF formulae for various boundary conditions and structural element dimensions by applying Castigliano's second theorem. Although they are originally derived for the cruciform joints, the SMF formulae can be converted into Eqs. (9) and (10) respectively accounting for axial misalignment and angular misalignment for a butt-welded joint under the test conditions depicted in Fig. 9, and assuming the specimen is symmetrically mounted between the fixtures.

$$K_{\mathrm{me}} = 1 + \left[-12\left(\frac{L_c}{L_f}\right)^3 + 18\left(\frac{L_c}{L_f}\right)^2 + 1.8\left(\frac{L_c}{L_f}\right) - 0.9\right] \bullet \frac{e}{t} \tag{9}$$

$$K_{\mathrm{m\alpha}} = 1 + \left[24\left(\frac{L_c}{L_f}\right)^4 - 48\left(\frac{L_c}{L_f}\right)^3 + 31.2\left(\frac{L_c}{L_f}\right)^2 - 7.2\left(\frac{L_c}{L_f}\right) + 0.8\right] \bullet \frac{L_f \bullet \alpha}{t} \tag{10}$$

in which L_c represents the distance from the critical location under investigation and the edge of the movable clamping fixture (see Fig. 9 for L_{c1} to L_{c4} corresponding to toe #1 to toe #4).

It is worth noting that the two sets of formulae mentioned above do not distinguish between the concave and convex sides of a distorted butt-welded joint. For the majority of specimens in the present study, as indicated in Table 1 and Table 2, the weld toe radii are smaller on the convex side compared to the concave side, and the weld flank angles are

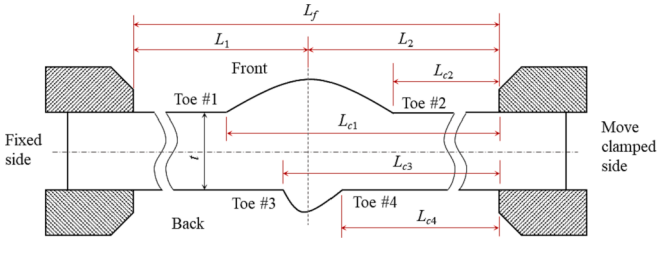

Fig. 9. The configuration of a butt-welded joint under clamping condition.

larger. This means that the stress concentration induced by the weld geometry would be more serious for the convex side. When axially straightening a butt-welded joint with angular misalignment, the concave and convex sides would experience positive and negative bending stresses, respectively. If one directly applies the SMFs from Eqs. (7) to (10), which are always larger than 1.0, without distinguishing the concave and convex sides, the local stress at the convex weld toes might be significantly overestimated. Therefore, based on finite element analysis results, Luo et al. [21] proposed Eq. (11) to increase the local stress at the concave side weld toes, while utilizing '2 - $K_{m\alpha}$' to decrease the local stress at the convex side weld toes, in order to account for the angular misalignment effect. Furthermore, according to the finite element results presented in [19,21], the local stress induced by axially straightening of a butt-welded joint with axial misalignment would be tensile at weld toe #1 and #4, while it would be compressive at weld toe #2 and #3 (refer to Fig. 9 for weld toe numbering). Consequently, Luo et al. [21] proposed Eq. (12) to account for the axial misalignment effect. The coefficients (C_1, C_2, and C_3) for each weld toe, as listed in Table 4, were obtained through regression analysis using a large amount of finite element results.

$$K_{m\alpha} = 1 + 5.582 \bullet \alpha \bullet \left(\ln\left(L_f/2t\right) - 1.2\right) \tag{11}$$

$$K_{me} = 1 + C_1 \bullet \left(\frac{e}{t}\right) \bullet \left(\ln\left(L_f/2t\right)^{C_2} + C_3\right) \tag{12}$$

In the case of the butt-welded joints containing both angular and axial misalignments, both K_{me} and $K_{m\alpha}$ should be applied using the following equation [14]:

$$K_m = 1 + (K_{me} - 1) + (K_{m\alpha} - 1) \tag{13}$$

3.3. SCF formulae

As previously presented in Section 2.3, fatigue cracks in all the fractured specimens were observed to originate at the weld toe. The weld toe SCF can be determined either directly by using the finite element method or using the approximate formulae available in the literature. Some representative SCF formulae that would be used for the following fatigue evaluation are briefly introduced here.

A simple and straightforward SCF formula for the butt-welded joint under axial loading has been proposed depending on only the weld toe radius (normalized by plate thickness) and flank angle by Lawrence and Ho [28,42], as in the form of Eq. (14). It is important to note that the weld reinforcement height (h) and width (w) have not been included in the formulae, because they assumed a relationship of $h/w = 0.5 \cdot \tan(0.5 \cdot \theta)$ for the weld reinforcement profile. Meanwhile, the investigated parameters include flank angles ranging from 15° to 60° and weld toe radii from approximately 0.5 mm to 3.8 mm.

$$K_{t\_Lawrence} = 1 + 0.27 \bullet \tan(\theta)^{0.25} \bullet \left(\frac{r}{t}\right)^{-0.5} \tag{14}$$

Pachoud et al. [29] proposed a SCF formula in a similar form but included the effect of weld reinforcement height, as shown in Eq. (15). The equation was derived through a parametric finite element analysis, which covered a wide range of weld geometrical parameters. They included flank angles ranging from 5° to 30°, weld toe radii from 0.4 mm to 1.9 mm, relative weld reinforcement heights (h/t) from 0.04 to 0.1, steel plate thicknesses from 20 mm to 50 mm, and relative reinforcement widths (w/t) ranging from approximately 0.73 to 1.38.

$$K_{t\_Pachoud} = 1 + 1.16\left(\frac{h}{t}\right)^{0.23} \bullet \tan\left(\frac{\theta}{2}\right)^{0.46} \bullet \left(\frac{r}{t}\right)^{-0.38} \tag{15}$$

Kiyak et al. [43] proposed an extended parametric SCF formula covering the wider weld toe radius from 0.1 mm to 4 mm and flank angle from 10° to 60°. However, it is important to note that the relative weld reinforcement height (h/t) is limited to 0.075 and 0.25, and the relative weld reinforcement width (w/t) is fixed at 1.46. Therefore, Luo et al. [30] modified this SCF formula into the form of Eq. (16) by extending the application ranges of the relative weld reinforcement height and width to 0.05 to 0.4 and 1.0 to 2.0, respectively.

$$K_{t\_Luo} = 1 + p_1\left(\frac{h}{t}\right)^{p_2\theta} \bullet \theta^{p_3} \bullet \exp(-p_4\theta) \bullet \left(\frac{r}{t}\right)^{-0.288\theta} \bullet \left(1 + \frac{\rho}{t}\right)^{-p_5} \bullet \left(p_6\left(\frac{h}{t}\right)^2 + p_7 \bullet \left(\frac{h}{t}\right) + p_8\right) \tag{16}$$

in which p_1 to p_8 are coefficients determined through regression analysis based on a large dataset obtained from finite element analysis, as listed in Table 5.

Notably, Eqs. (15) and (16) do not include the relative weld reinforcement width (w/t) term. This omission is based on their finite element results, which indicated a negligible effect for the investigated range of $0.73 < w/t < 2.0$ [29,30]. In the case of back side welds in the current study, their relative reinforcement widths are as small as 0.34 to 0.6 (see Table 2). In [27], Remes and Varsta proposed the SCF formulae as shown in Eq. (17), in which the term of w/t is included. This equation is suitable for both arc and laser butt-welded joints, despite the latter joint having much smaller and sharper weld beads compared to the former. This suitability arises because their parametric study covered flank angles ranging from 5° to 100°, weld toe radii from 0.04 mm to 1.6 mm, relative weld reinforcement heights up to 0.21, and relative reinforcement widths ranging from approximately 0.08 to 1.67.

$$K_{t\_Remes} = 1 + \left(\frac{h}{t}\right)^{0.3} \bullet \left(\frac{w}{t}\right)^{0.3} \bullet \sin\left(\frac{\theta}{2}\right)^{0.3} \bullet \left(\frac{r}{t}\right)^{-0.32} \tag{17}$$

3.4. Fatigue crack location prediction

The initial step for fatigue evaluation of a weld joint is to identify the location where a fatigue crack is most likely to originate. As indicated in Table 1 and Table 2, there are notable differences in weld geometry, especially in weld toe radius and weld flank angle, among the four weld toes of the investigated butt-welded joints. In addition, the axially straightening of a butt-welded joint with axial and angular misalignments would introduce tensile or compressive local stress at different weld toes [19,21]. In such cases, the combined effects of weld geometry and misalignment make all four weld toes potential candidates for fatigue crack initiation according to their competitive nature. With the weld geometries and misalignments measured in Section 2.2, the local stresses at the weld toes can be calculated by incorporating the SMF and SCF formulae introduced in Sections 3.2 and 3.3, respectively, with Eq. (6).

Figs. 10, 11, 12 present the results of the predicted fatigue crack location of each specimen, assuming that the fatigue crack is most likely to initiate at the weld toe where the highest local stress is observed. These histogram figures display the highest K_{mt} values among all four weld toes on the horizontal axis and the specimen IDs on the vertical axis, while distinguishing fatigue crack locations with various filled colors and patterns. Here, K_{mt} is the product of SMF and SCF, as indicated in Eq. (6), which includes the combined effects of both misalignments and weld geometries.

Fig. 10 shows the prediction results based on the SMF formulae of IIW Recommendation [14] (i.e., Eqs. (7) and (8)) combined with various

Table 4
Coefficients of Equation (12) [21].

Coefficients	Front side		Back side	
	Toe #1	Toe #2	Toe #3	Toe #4
C_1	24.407	1.152	1.345	21.720
C_2	0.030	−2.607	−1.646	0.027
C_3	−0.923	−1.946	−1.772	−0.904

Table 5
Coefficients of Eq. (16) [30].

Coefficient	p_1	p_2	p_3	p_4	p_5	p_6	p_7	p_8
Value	1.398	−0.144	0.715	1.650	0.322	−2.233	2.319	0.526

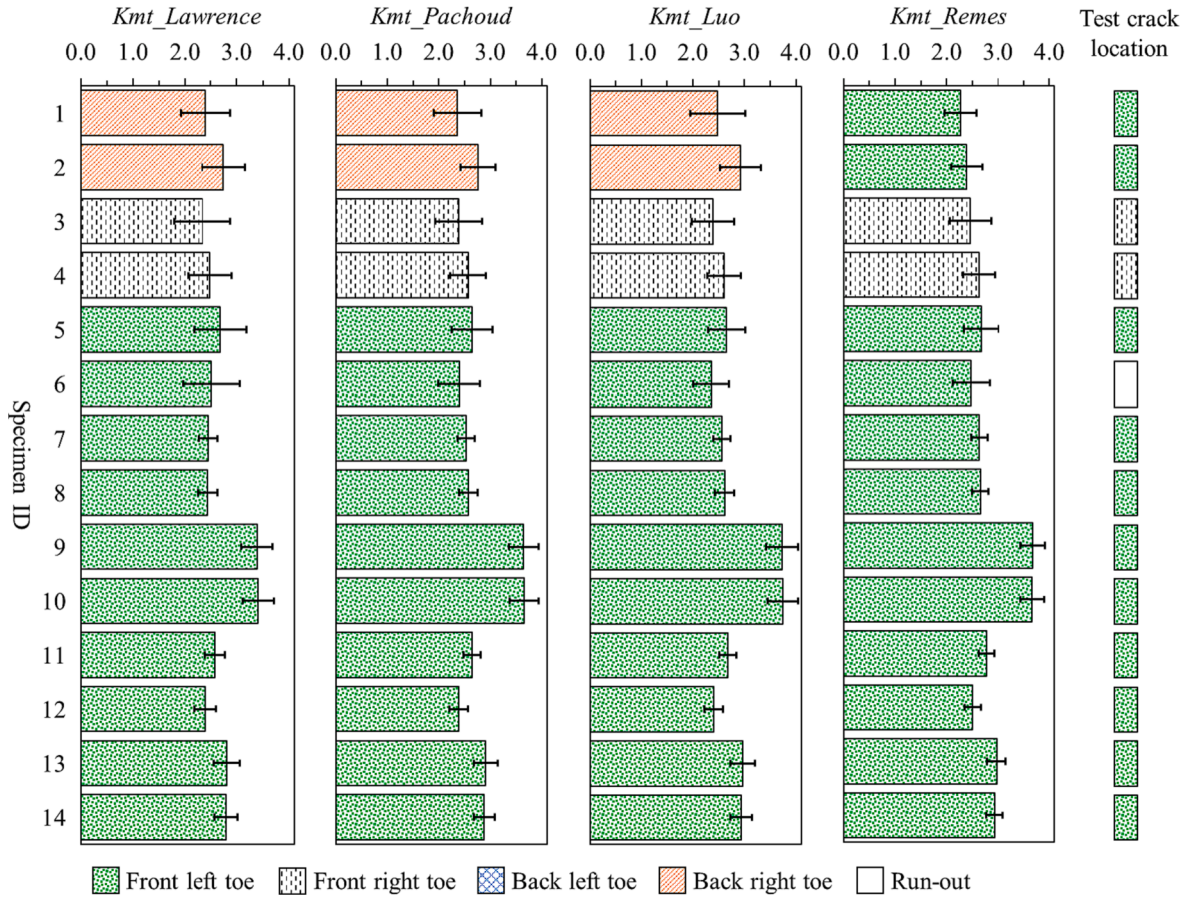

Fig. 10. Prediction for fatigue crack location using modified IIW SMF formulae in combination with various SCF formulae.

SCF formulae described in Section 3.3. It should be noted that the original IIW SMF formulae, which do not differentiate between concave and convex sides or account for secondary bending induced positive or negative local stresses at different weld toes, have been modified following the observations from [21]. In cases of positive axial misalignment, Eq. (7) is applied to increase the local stress at weld toes #1 and #4, while '2 - K_{me}' is utilized to decrease the local stress at weld toes #2 and #3 (refer to Fig. 9 for weld toe numbering). For angular misalignment, Eq. (8) is used to increase the local stress at the concave side weld toes, while '2 - $K_{m\alpha}$' is employed to decrease the local stress at the convex side weld toes. As shown, all the SCF formulae give the same prediction results for fatigue crack location, except for specimens 1 and 2. For these two specimens, the predicted fatigue crack locations according to the SCF formulae of Lawrence and Ho, Pachoud et al., and Luo et al., all fall into weld back side, inconsistent with the observations from the tests. This is mainly because, on one hand, the angular misalignments of these two specimens are relatively small compared to others (see Table 3). On the other hand, as indicated in Tables 1 and 2, the weld toes on the back side have smaller radii and larger flank angles than those on the front side. The combined effects of above-mentioned two factors make K_t dominant over K_m. However, it is noteworthy that for the SCF formula of Remes and Varsta, the predicted fatigue crack locations are consistent with the experimental observations for all specimens, revealing the necessity of considering the effect of weld reinforcement width.

Fig. 11 shows the prediction results based on the SMF formulae proposed by Xing and Dong [16] (i.e., Eqs. (9) and (10)), which have been modified in the same manner as applied to the IIW SMF formulae. It is obvious that the predicted fatigue crack locations based on the modified SMF formulae of Xing and Dong are almost the same as those predicted by the modified IIW SMF formulae. The prediction results according to the SMF formulae proposed by Luo et al. [21] (i.e., Eqs. (11) and (12)) are presented in Fig. 12. Notably, in contrast to the results that obtained by incorporating with the SMF formulae of IIW (see Fig. 10) and Xing and Dong (see Fig. 11), the predicted fatigue crack locations based on the SCF formulae of Lawrence and Ho, Pachoud et al., and Luo et al., mostly fall into weld back sides. The main reason for this discrepancy is that, as shown in Fig. 13, the difference between the K_m values of the front left and back right weld toes is significantly smaller when calculated using the SMF formulae of Luo et al., compared to those obtained from the other two sets of SMF formulae. Under such circumstances, the higher K_t values resulting from the smaller radii and larger flank angles of back right weld toes (see Table 1 and Table 2) lead to the highest K_{mt} values among four weld toes. Nevertheless, Remes and Varsta's SCF formulae still accurately predicts fatigue crack locations for all specimens consistent with the experimental observations. This further demonstrates the crucial role of weld reinforcement width in predicting the fatigue crack location, particularly in the case of narrower

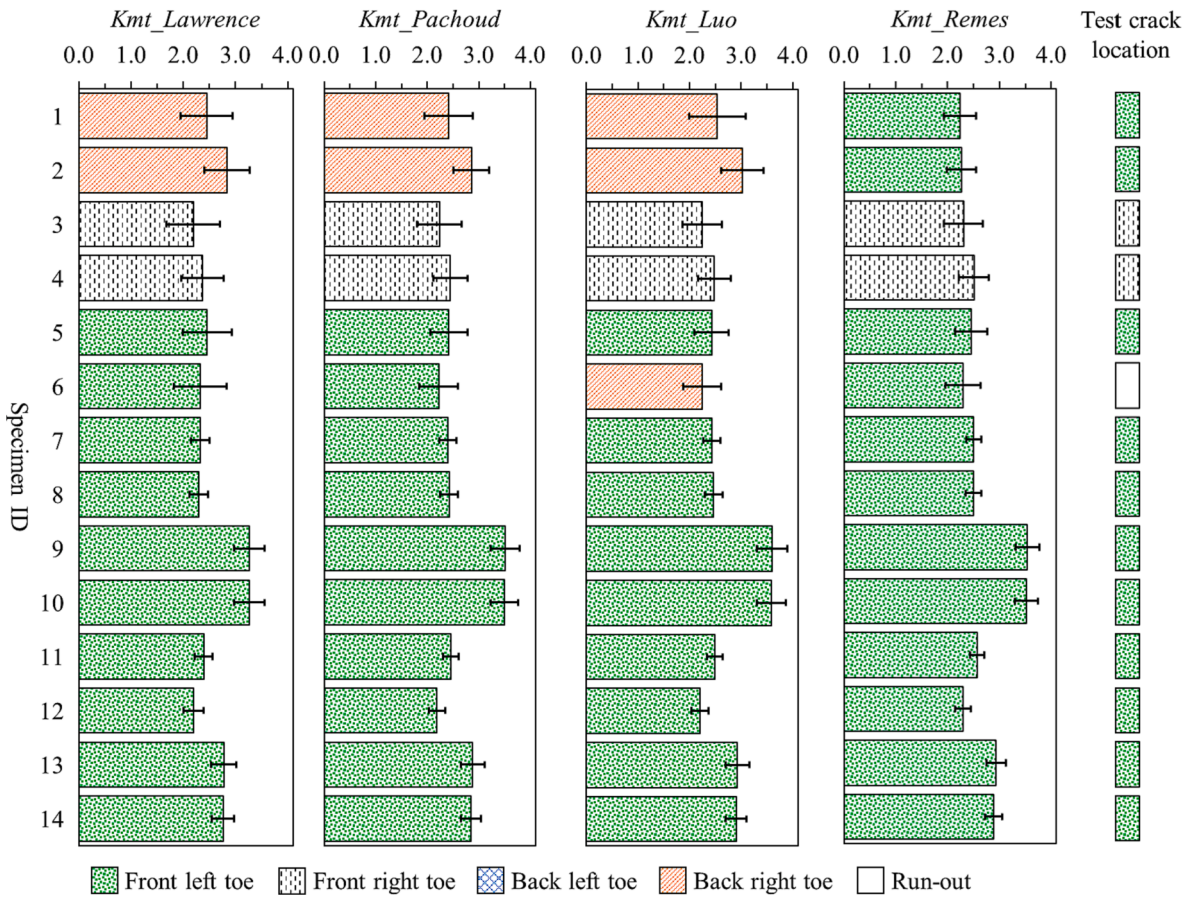

Fig. 11. Prediction for fatigue crack location using modified Xing and Dong's SMF formulae in combination with various SCF formulae.

welds with small relative reinforcement width (w/t). In this sense, among the four SCF formulae introduced in Section 3.3, Remes and Varsta's SCF formula (i.e., Eq. (17)), which includes the weld reinforcement width term and covers a wide range of $0.08 < w/t < 1.67$, proves to be the most suitable for evaluating fatigue crack locations in one-side full penetration butt-welded joints.

Fig. 14 displays the fracture surfaces of representative specimens with easily identifiable crack initiation sites along the weld length, along with the K_{mt} distribution computed using Luo et al.'s SMF formulae and Remes and Varsta's SCF formulae. It is not surprising that the K_{mt} values vary significantly along the weld length due to the significant variations in the measured weld geometrical parameters (see Fig. 4). Nevertheless, the notably different *Kmt* between the left and right weld toes for specimens 7 and 12, as shown in Fig. 14(c) and Fig. 14(d), is due to the combined effect of axial misalignment and weld geometries. Firstly, the secondary bending stress induced by axial misalignment would be tensile and compressive on the left and right weld toes, respectively [19,21], resulting in $K_m > 1.0$ and $K_m < 1.0$ for the corresponding weld toes. Secondly, as indicated in Table 1, the left weld toes have smaller radii and larger flank angles than the right weld toes for both specimens 7 and 12, resulting in larger K_t on the left weld toes. Obviously, all the investigated specimens fractured due to fatigue cracks originating from the weld toes that with a larger average K_{mt}. However, it is worth noting that the distribution of K_{mt} along the weld length does not appear to be closely related to the crack initiation sites. This is most likely because the effects of welding induced defects, such as undercut, which play an important role in crack initiation sites [35], are not accounted for in the current K_{mt}.

3.5. Fatigue strength evaluation

The fatigue test data for all the studied butt-welded joints in Table 3 is assessed using S-N curves plotted in a log–log scale. Fig. 15 shows the fatigue test data in both the nominal stress range ($\Delta\sigma$) applied during testing and the modified stress range ($\Delta\sigma_m$), which incorporates misalignment modifications through various SMF formulae. For comparison, the S-N curves specified in the JSSC specification and IIW recommendations are plotted alongside the S-N curves that are derived using regression analysis. Note that the intercept term of Eq. (18), denoted as log$C$, is determined under both fixed slope (i.e., $m = 3$) and free slope conditions, with excluding the data points of 'run-out' from the regression analysis.

$$logN = logC - m{\cdot}log\Delta\sigma \tag{18}$$

From Fig. 15(a), it can be observed that all specimens are above JSSC-F (65 MPa at 2 million cycles) and IIW FAT71 (71 MPa at 2 million cycles) S-N curves. These curves are nominal stress-based and are typically applied to transversely loaded one-side full penetration butt-welded joints without a backing plate. This implies that even without explicit consideration of any misalignment effects, the FAT71 S-N curve, which has already covered a SMF of $K_m = 1.15$ [14], still yields a conservative estimate for fatigue strength. Meanwhile, the test data in terms of nominal stress range exhibit significant scatter, as evidenced by the standard deviation of log$C$, which is 0.35 for both fixed and free slope regression methods. After applying misalignment modification according to Eq. (19), with K_m calculated based on the measured average axial and angular misalignments from Table 3, the scatter in the data significantly reduces, leading to a narrower discrete band as shown in Fig. 15 (b) to Fig. 15 (d). This is also supported by a notable decrease in the standard deviations of log$C$ to 0.19, 0.18, and 0.22 for the SMF formulae

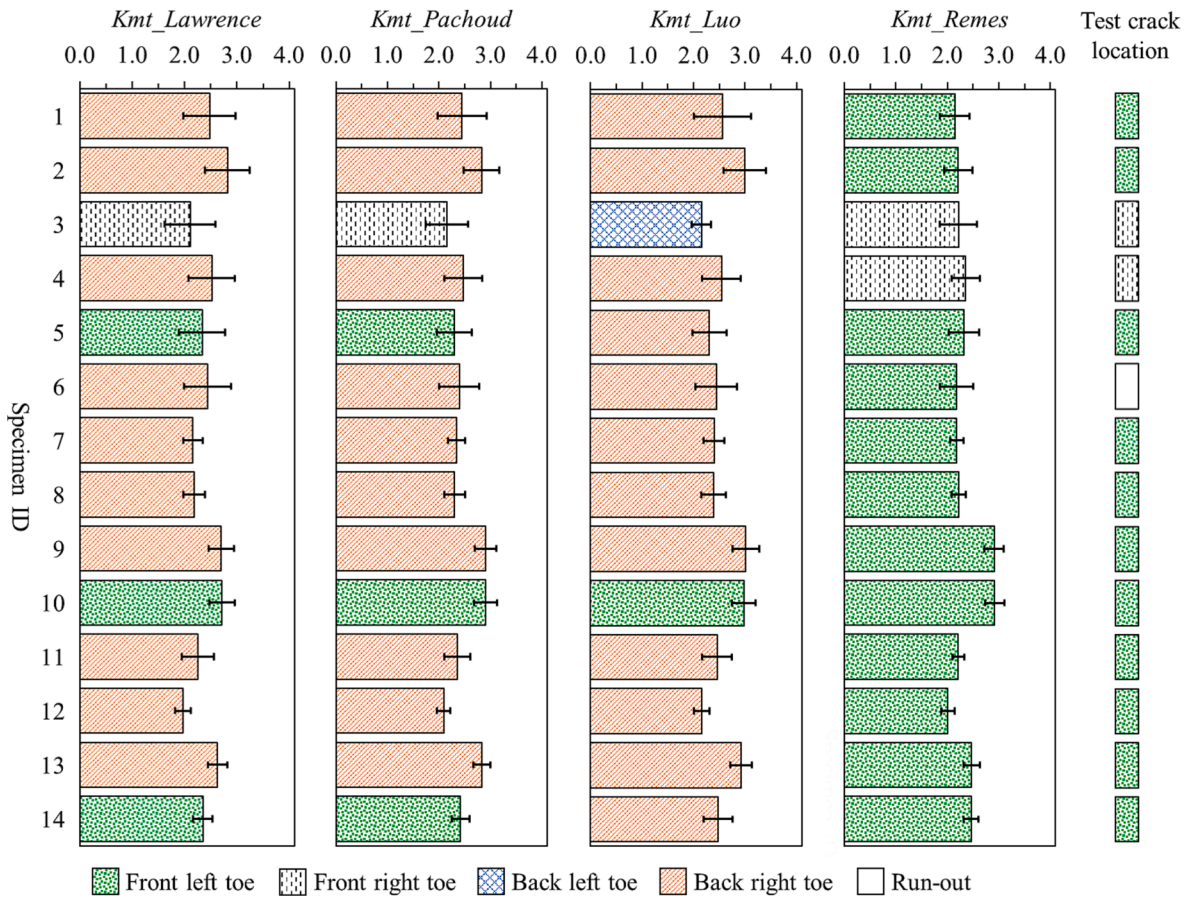

Fig. 12. Prediction for fatigue crack location using Luo et al.'s SMF formulae in combination with various SCF formulae.

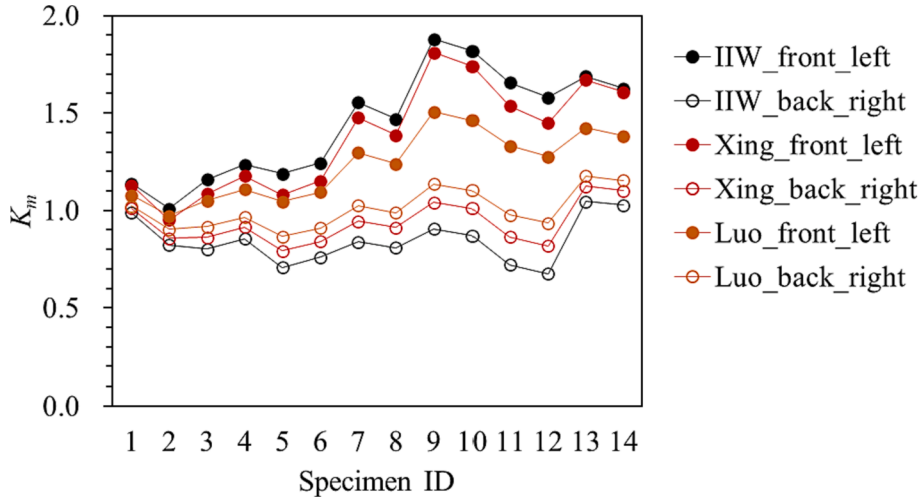

Fig. 13. K_m calculated by different SMF formulae.

of IIW Recommendation [14], Xing and Dong [16], and Luo et al. [21], respectively, when using the fixed slope regression method. Moreover, the derived slopes are $m = 4.56$, 4.54, and 6.12, with the corresponding standard deviations of log$C$ further decreasing to 0.15, 0.14, and 0.14 when using the free slope regression method. These results demonstrate that the misalignments are critical factors for determining the fatigue life of butt-welded joints. Additionally, the JSSC-B (155 MPa at 2 million cycles) and IIW FAT112 (112 MPa at 2 million cycles) S-N curves, recommended for the transverse loaded butt-welded joint with the weld reinforcement part ground flush to plate by JSSC specification [15], and IIW recommendations [14], respectively, are also plotted in the plots for comparison purpose. It can be observed that the data points fall on both sides of the JSSC-B curve, while all of them fall above the IIW FAT112 curve. This suggests that even without explicitly considering any weld geometry effects, the IIW FAT112 curve still provides a conservative estimate for fatigue life, given that the weld geometry induced SCF is $K_t = 1.0$ in case of the ground flush butt-welded joints.

$$\Delta\sigma_m = K_m \bullet \Delta\sigma \tag{19}$$

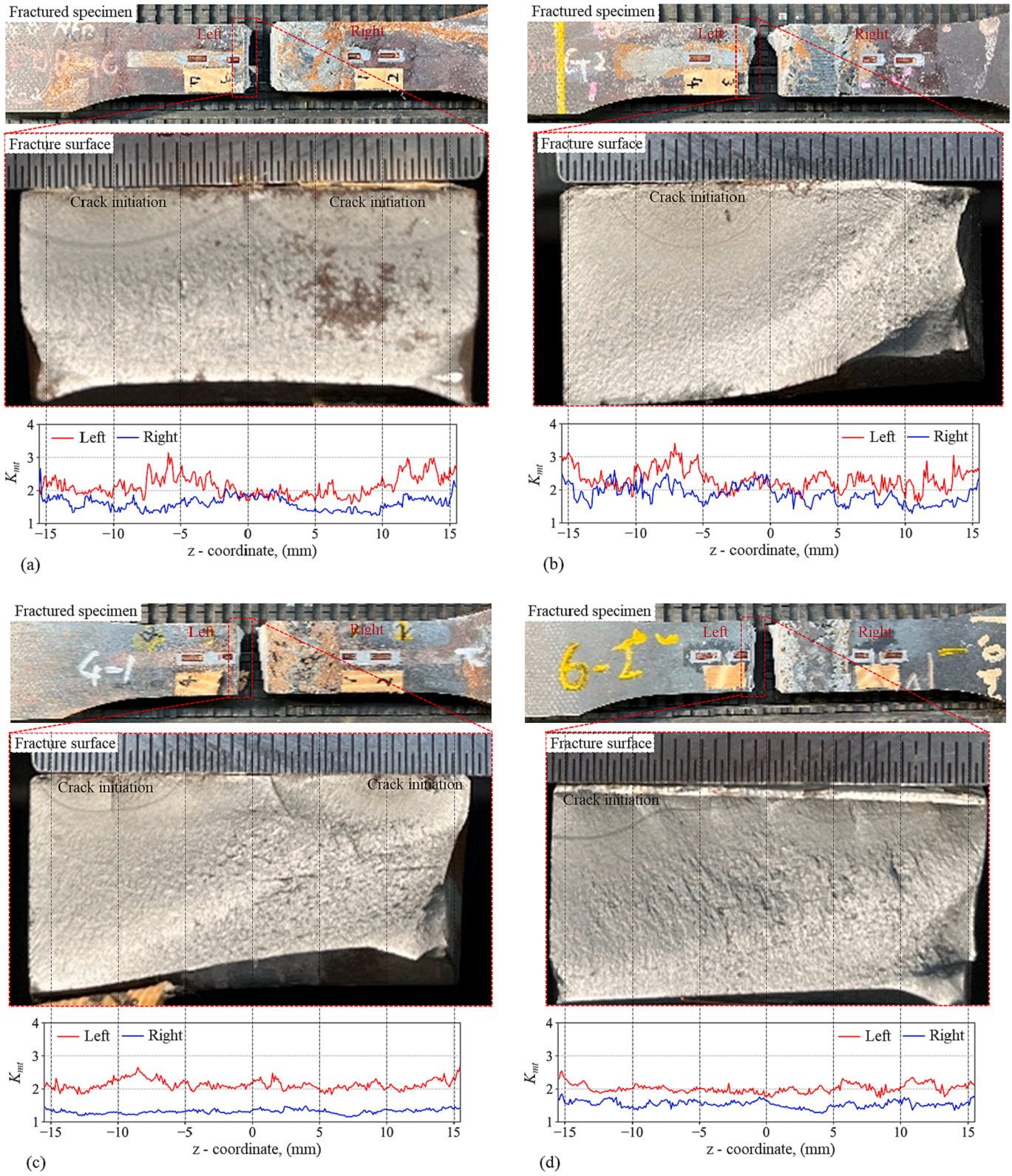

Fig. 14. Crack initiation sites plot with K_{mt} distribution along weld length for representative specimens: (a) specimen 1; (b) specimen 5; (c) specimen 7; (d) specimen 12.

To further examine the effects of weld geometrical parameters on fatigue life prediction, Fig. 16 to Fig. 18 present the fatigue data in terms of the local stress ranges ($\Delta\sigma_{mt}$), which are calculated using Eq. (20). Since the surfaces of specimens 1 to 6 were powder coated while specimens 7 to 14 were lacquer sprayed for enhancing reflectivity of optical measurement (Section 2.2.1). It is observed in Table 1 and Table 2 that the powder-coated specimens (1 to 6), on average, exhibit smaller weld toe radii compared to the lacquer-sprayed specimens (7 to 14), resulting in larger SCF for powder-coated specimens as shown in Figs. 16, 17, 18. Consequently, it is important to note that the fatigue data have been

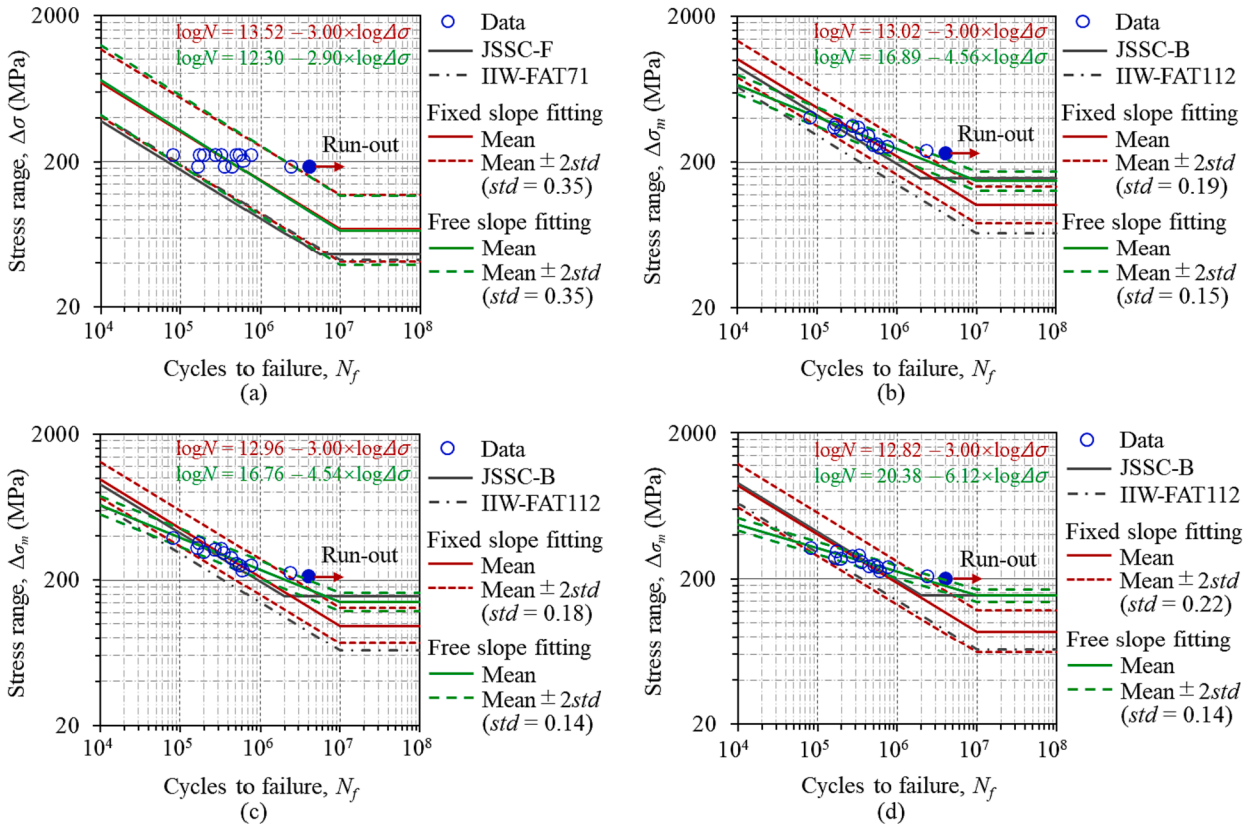

Fig. 15. Fatigue test data plotting with the S-N curves: (a) nominal stress range; (b) misalignment modification by IIW SMF; (c) misalignment modification by Xing and Dong's SMF; (d) misalignment modification by Luo et al.'s SMF.

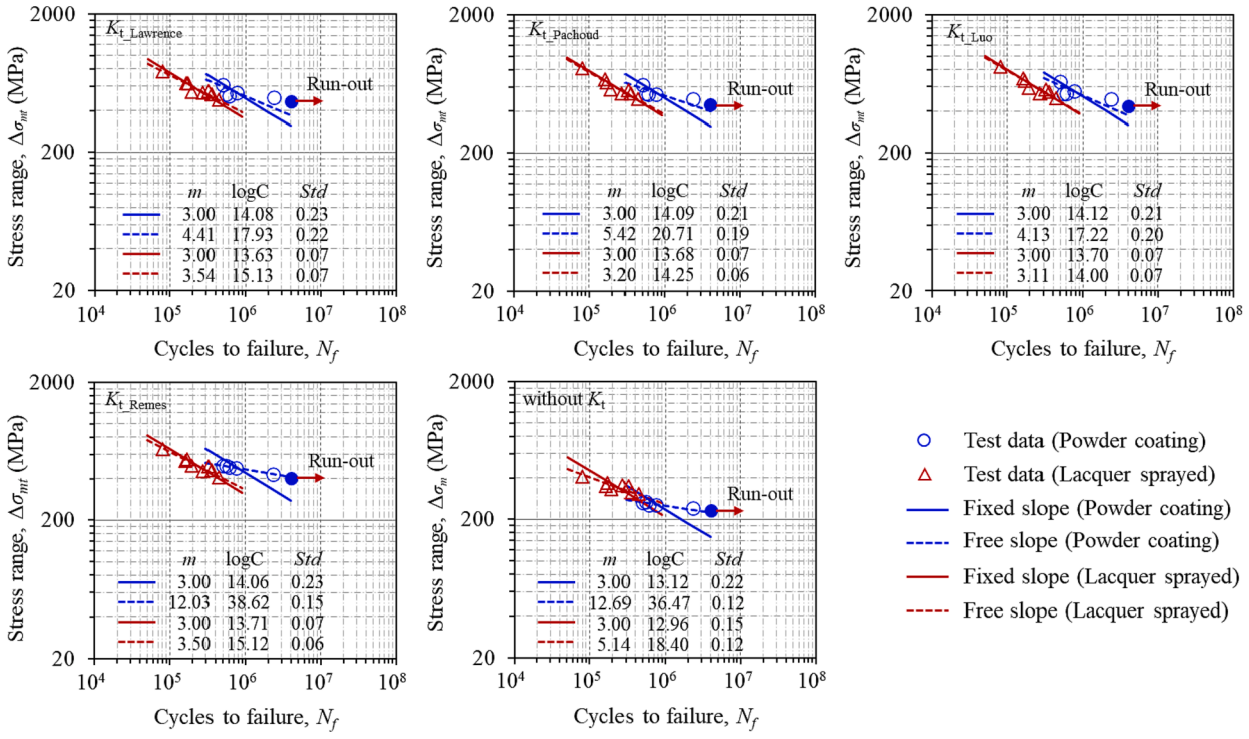

Fig. 16. Test data plot in local stress range with misalignment correction by IIW SMF.

categorized into two groups in the subsequent regression analysis. Meanwhile, the intercept term log$C$ is determined under both fixed slope (i.e., $m = 3$) and free slope conditions, excluding the data points of 'run-out' from the regression analysis.

$$\Delta\sigma_{mt} = K_{mt} \bullet \Delta\sigma = K_m \bullet K_t \bullet \Delta\sigma \tag{20}$$

Fig. 16 shows the $\Delta\sigma_{mt}$-N results based on the SMF formulae of IIW Recommendation [14] (i.e., Eqs. (7) and (8)) combined with various SCF formulae. For powder-coated specimens, fixing $m = 3$ in regression results in standard deviations of log$C$, incorporating weld geometry effects through various SCF formulae, ranging between 0.21 and 0.23. This shows no significant difference compared to the observed value of 0.22 without considering SCF. However, including weld geometry effects in free slope regression leads to an increase in the standard deviations of log$C$, with Lawrence and Ho's SCF formulae showing the most notable rise from 0.12 to 0.23. For lacquer-sprayed specimens, whether in fixed slope or free slope regression, a notable decrease in the standard deviations of log$C$ is observed upon incorporating weld geometry effects through various SCF formulae. Specifically, the values decrease from 0.15 to 0.07 for fixed slope condition and from 0.12 to 0.06 for free slope condition when compared to the cases without considering SCF.

Fig. 17 shows the results based on the SMF formulae proposed by Xing and Dong [16] (i.e., Eqs. (9) and (10)). Similarly, for powder-coated specimens, incorporating weld geometry effects through various SCF formulae does not result in a significant difference in the standard deviations of log$C$ compared to that observed without considering SCF when fixing $m = 3$ in regression. Nonetheless, it is observed that including weld geometry effects through Remes and Varsta's SCF formulae in free slope regression results in a notable decrease in standard deviations of log$C$ (from 0.17 to 0.05), while the other three sets of SCF formulae still lead to an increase in the standard deviations of log$C$. For lacquer-sprayed specimens, when compared to the cases without considering SCF, the standard deviations of log$C$ decrease from 0.14 to 0.08 for fixed slope condition and from 0.12 to 0.08 for free slope condition after incorporating weld geometry effects.

The results according to the SMF formulae proposed by Luo et al. [21] (i.e., Eqs. (11) and (12)) are presented in Fig. 18. For powder-coated specimens, the impact of considering the weld geometry effects on the standard deviation of log$C$ is similar to the corresponding results based on the SMF formula proposed by Xing and Dong (see Fig. 17). For lacquer-sprayed specimens, a notable decrease in the standard deviations of log$C$ is observed only when incorporating weld geometry effects through Remes and Varsta's SCF formulae. Compared to the cases without considering SCF, standard deviations decrease from 0.15 to 0.08 for fixed slope and from 0.13 to 0.07 for free slope conditions.

4. Conclusions

Fourteen one-side full penetration butt-welded joints are fabricated under various specified assembly root gaps and axial eccentricities, and then tested under cyclic tensile loading with constant amplitude. Misalignments and weld geometries are also measured using a 3D optical scanning system and then being employed for fatigue behavior evaluation using several SMF and SCF formulae available in the literature. Based on the investigations, the following conclusions can be drawn:

(1) The measured axial misalignments range from −0.45 mm to 2.09 mm, exhibiting a strong positive correlation with the assembled axial eccentricities. Angular misalignments ranging from 0.46° to 2.98° are observed in all specimens. A correlation coefficient of 0.719 indicates a positive correlation between the angular misalignments and the axial misalignments. The fatigue test results indicate a noticeable decrease in nominal stress fatigue strength as the assembled axial eccentricities increase, regardless of the assembled root gaps. This decrease is primarily attributed to the secondary bending stress effect induced by the misalignments.

(2) On one hand, there is a strong negative correlation between the assembled root gap and the ratio of weld reinforcement height to width (i.e., h_f / w_f and h_b / w_b) for both the weld front and back sides, with correlation coefficients of −0.883 and −0.877, respectively. This indicates that a larger assembled root gap corresponds to a flatter weld reinforcement, which is beneficial for fatigue strength improvement. However, on the other hand, a correlation coefficient of 0.499 between RG and α suggests a potential increase in angular misalignment with a larger assembled root gap, leading to a reduction in fatigue strength.

(3) The weld geometry measurement results indicate that smaller but steeper weld profiles are formed on the back side of specimens.

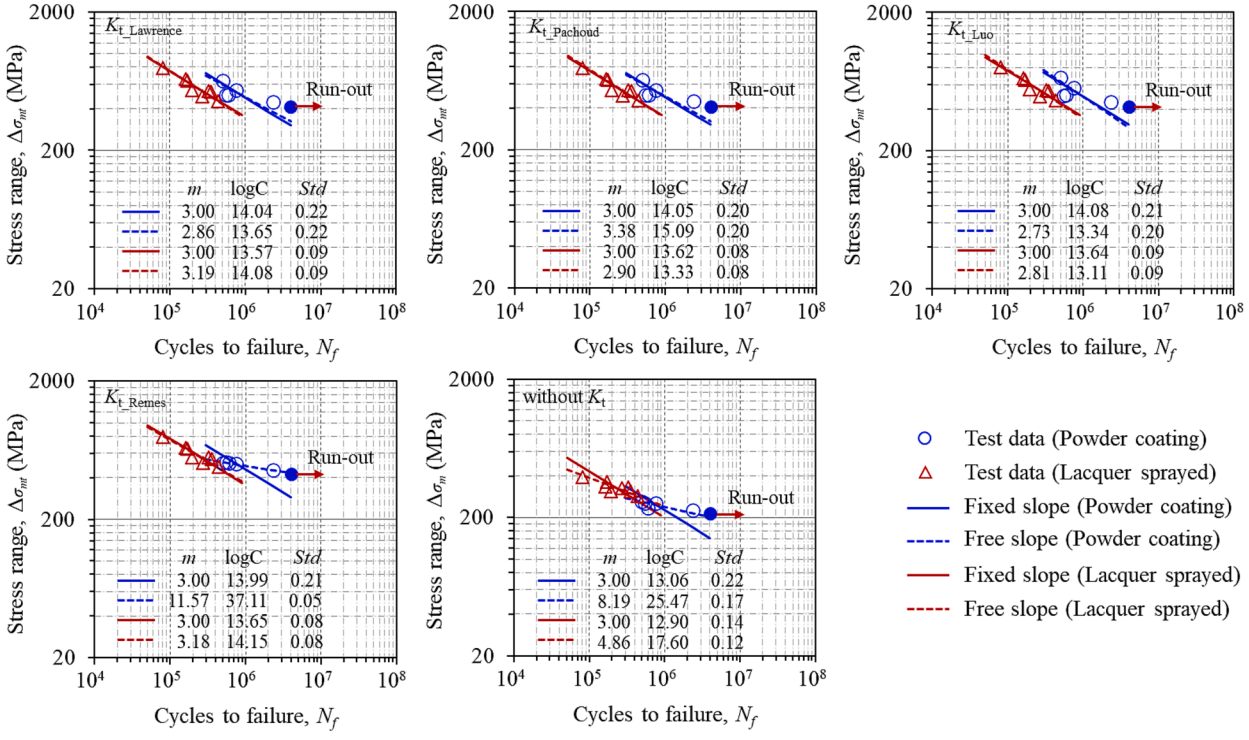

Fig. 17. Test data plot in local stress range with misalignment correction by Xing and Dong's SMF.

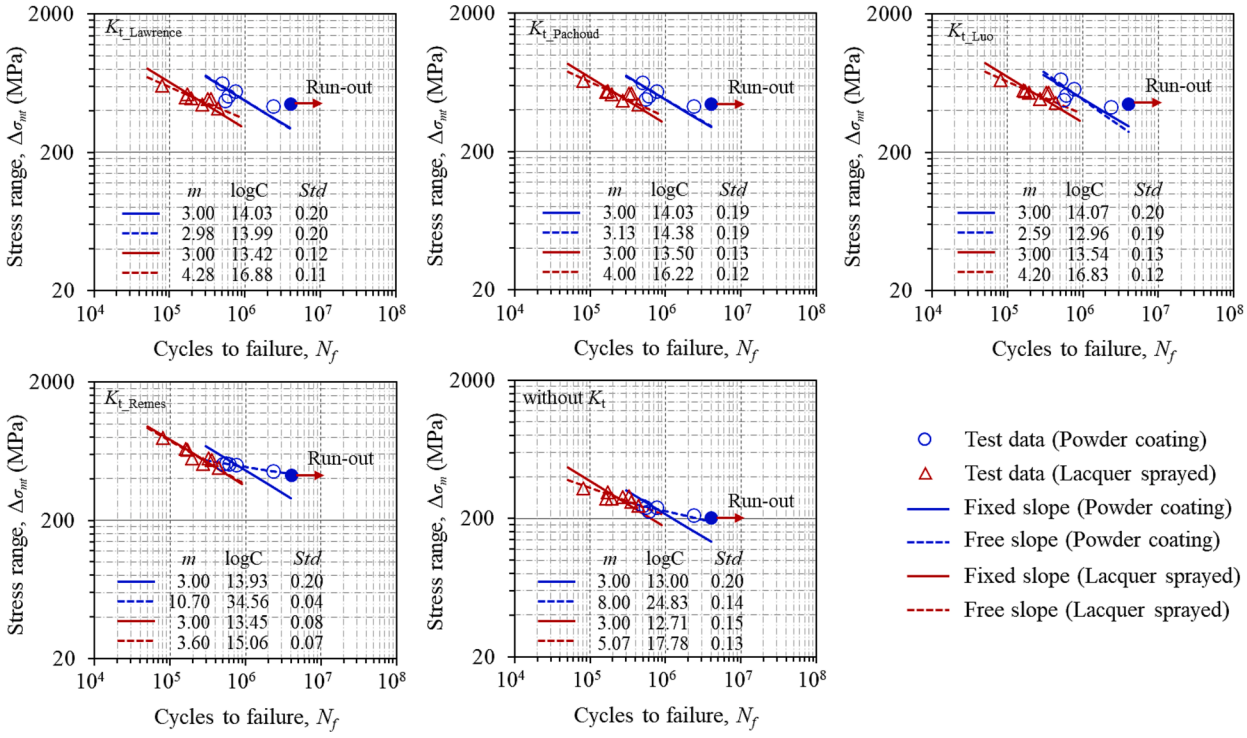

Fig. 18. Test data plot in local stress range with misalignment correction by Luo et al.'s SMF.

The average values of weld toe radius and flank angle vary significantly between specimens, as well as between the left and right weld toes, and also between the weld front side and weld back side. On average, the powder-coated specimens have smaller weld toe radii compared to the lacquer-sprayed specimens. Regardless of the combined SMF formula, among the four mentioned formulae in Section 3.3, Remes and Varsta's SCF formula (i.e., Eq. (17)) is the only one that accurately predicts fatigue crack locations for all specimens and is consistent with the experimental observations. This is mainly because it includes the weld reinforcement width term and covers a wide range of $0.08 < w/t < 1.67$.

(4) The test data initially in terms of nominal stress range exhibit a high degree of scatter with a standard deviation of 0.35 for log$C$. The corresponding standard deviations decrease to 0.18 ~ 0.22 and 0.14 ~ 0.15 for fixed slope and free slope regression conditions, respectively, after accounting for misalignment correction using various SMF formulae. The standard deviations of log$C$ further decrease to as small as 0.04 ~ 0.08 when incorporating weld geometry effects through Remes and Varsta's SCF formulae. These results demonstrate combined effects of misalignments and weld geometries on fatigue strength of investigated butt-welded joints.

(5) Due to its outstanding accuracy and robustness in evaluating both the fatigue crack location and fatigue life for the investigated butt-welded joints, the combination of Remes and Varsta's SCF formula with Luo et al.'s SMF formula is the most recommended method for the one-side full penetration butt-welded joints. However, the general applicability of the proposed method should be further confirmed through additional test results, as the current study is limited by the number of specimens.

CRediT authorship contribution statement

Pengjun Luo: Conceptualization, Investigation, Validation, Writing – original draft. **Yuta Mashino:** Data curation, Resources. **Yuki Matsuo:** Data curation, Resources. **Yuki Kasaoka:** Data curation, Resources. **Seiichiro Tsutsumi:** Conceptualization, Project administration, Writing – review & editing.

Declaration of competing interest

The authors declare that they have no known competing financial interests or personal relationships that could have appeared to influence the work reported in this paper.

Data availability

Data will be made available on request.

Acknowledgment

Financial support from the Japan Society for the Promotion of Science (JSPS), No. 21H01545 and No. 23KF0050, is especially acknowledged.

References

[1] Vukelic G, Vizentin G, Brnic J, Brcic M, Sedmak F. Long-term marine environment exposure effect on butt-welded shipbuilding steel. J Mar Sci Eng 2021;9. https://doi.org/10.3390/jmse9050491.

[2] Su H, Wang J, Du J. Fatigue behavior of uncorroded butt welded joints made of bridge weathering steel. Structures 2020;24:377–85. https://doi.org/10.1016/j.istruc.2020.01.032.

[3] Petry A, Gallo P, Remes H, Niemelä A. Optimizing the Voce-Chaboche Model Parameters for Fatigue Life Estimation of Welded Joints in High-Strength Marine Structures. J Mar Sci Eng 2022;10. https://doi.org/10.3390/jmse10060818.

[4] Zhao X, Fan Y, Liu Y, Wang H, Dong P. Evaluation of fatigue fracture mechanism in a flash butt welding joint of a U75V type steel for railroad applications. Eng Fail Anal 2015;55:26–38. https://doi.org/10.1016/j.engfailanal.2015.05.001.

[5] Deng D, Murakawa H. Prediction of welding distortion and residual stress in a thin plate butt-welded joint. Comput Mater Sci 2008;43:353–65. https://doi.org/10.1016/j.commatsci.2007.12.006.

[6] Schork B, Kucharczyk P, Madia M, Zerbst U, Hensel J, Bernhard J, et al. The effect of the local and global weld geometry as well as material defects on crack initiation and fatigue strength. Eng Fract Mech 2018;198:103–22. https://doi.org/10.1016/j.engfracmech.2017.07.001.

[7] Molski KL, Tarasiuk P. Stress concentration factors for welded plate T-joints subjected to tensile bending, and shearing loads. Materials (Basel) 2021;14:1–22. https://doi.org/10.3390/ma14030546.
[8] Wahab MA, Sakano M. Experimental study of corrosion fatigue behaviour of welded steel structures. J Mater Process Technol 2001;118:116–21. https://doi.org/10.1016/s0924-0136(01)00902-5.
[9] Braun M, Kellner L. Comparison of machine learning and stress concentration factors-based fatigue failure prediction in small-scale butt- welded joints. Fatigue Fract Eng Mater Struct 2022;45:3403–17. https://doi.org/10.1111/ffe.13800.
[10] Nguyen NT, Wahab MA. The effect of undercut and residual stresses on fatigue behaviour of misaligned butt joints. Eng Fract Mech 1996;19:769–78. https://doi.org/10.1016/0013-7944(96)00024-0.
[11] Ferreira JM, Branco CM. Influence of misalignment on the fatigue strength of butt welds. Int J Fatigue 1991;13:405–9. https://doi.org/10.1016/0142-1123(91)90597-R.
[12] Fricke W, Remes H, Feltz O, Lillemäe I, Tchuindjang D, Reinert T, et al. Fatigue strength of laser-welded thin-plate ship structures based on nominal and structural hot-spot stress approach. Ships Offshore Struct 2013;10:39–44. https://doi.org/10.1080/17445302.2013.850208.
[13] Ottersböck MJ, Leitner M, Stoschka M, Maurer W. Analysis of fatigue notch effect due to axial misalignment for ultra high-strength steel butt joints. Weld World 2019;63:851–65. https://doi.org/10.1007/s40194-019-00713-4.
[14] Hobbacher A. Recommendations for fatigue design of welded joints and components 2016. https://doi.org/10.1007/978-3-319-23757-2.
[15] Japanese Society of Steel Construction. Fatigue design recommendations for steel structures. 1995.
[16] Xing S, Dong P. An analytical SCF solution method for joint misalignments and application in fatigue test data interpretation. Mar Struct 2016;50:143–61. https://doi.org/10.1016/j.marstruc.2016.07.006.
[17] Shen W, Qiu Y, Li C, Hu Y, Li M. Fatigue strength evaluation of thin plate butt joints considering initial deformation. Int J Fatigue 2019;125:85–96. https://doi.org/10.1016/j.ijfatigue.2019.03.036.
[18] Lillemäe I, Lammi H, Molter L, Remes H. Fatigue strength of welded butt joints in thin and slender specimens. Int J Fatigue 2012;44:98–106. https://doi.org/10.1016/j.ijfatigue.2012.05.009.
[19] Taras A, Unterweger H. Numerical methods for the fatigue assessment of welded joints: influence of misalignment and geometric weld imperfections. Eng Struct Technol 2017;9:9–24. https://doi.org/10.3846/2029882x.2017.1299968.
[20] Lillemäe I, Remes H, Liinalampi S, Itävuo A. Influence of weld quality on the fatigue strength of thin normal and high strength steel butt joints. Weld World 2016;60:731–40. https://doi.org/10.1007/s40194-016-0326-8.
[21] Luo Y, Tsutsumi S, Han R, Ma R, Dai K. Parametric formulae for stress concentration factor and clamping-induced stress of butt-welded joints under fatigue test condition. Weld World 2022;66:1897–913. https://doi.org/10.1007/s40194-022-01322-4.
[22] Arzola N, Hernández E. Experimental characterization of fatigue strength in butt welded joint considering the geometry and the effect of cooling rate of the weld. J Phys Conf Ser 2017;843:1–18. https://doi.org/10.1088/1742-6596/843/1/012047.
[23] Tsutsumi S, Fincato R, Luo P, Sano M, Umeda T, Kinoshita T, et al. Effects of weld geometry and HAZ property on low-cycle fatigue behavior of welded joint. Int J Fatigue 2022;156:106683. https://doi.org/10.1016/j.ijfatigue.2021.106683.
[24] Luo P, Zhang Q, Bao Y, Zhou A. Fatigue evaluation of rib-to-deck welded joint using averaged strain energy density method. Eng Struct 2018;177:682–94. https://doi.org/10.1016/j.engstruct.2018.09.090.
[25] Lee CH, Chang KH, Jang GC, Lee CY. Effect of weld geometry on the fatigue life of non-load-carrying fillet welded cruciform joints. Eng Fail Anal 2009;16:849–55. https://doi.org/10.1016/j.engfailanal.2008.07.004.
[26] Hultgren G, Mansour R, Barsoum Z. Fatigue strength assessment of welded joints incorporating the variability in local weld geometry using a probabilistic framework. Int J Fatigue 2023;167:1–13. https://doi.org/10.1016/j.ijfatigue.2022.107364.
[27] Remes H, Varsta P. Statistics of weld geometry for laser-hybrid welded joints and its application within notch stress approach. Weld World 2010;54:189–207. https://doi.org/10.1007/BF03263505.
[28] Yung J-Y, Lawrence FV. Analytical and graphical aids for the fatigue design of weldments. Fatigue Fract Eng Mater Struct 1985;8:223–41. https://doi.org/10.1111/j.1460-2695.1985.tb00424.x.
[29] Pachoud AJ, Manso PA, Schleiss AJ. New parametric equations to estimate notch stress concentration factors at butt welded joints modeling the weld profile with splines. Eng Fail Anal 2017;72:11–24. https://doi.org/10.1016/j.engfailanal.2016.11.006.
[30] Luo Y, Ma R, Tsutsumi S. Parametric formulae for elastic stress concentration factor at the weld toe of distorted butt-welded joints. Materials (Basel) 2020;13:1–19. https://doi.org/10.3390/ma13010169.
[31] Braun M, Neuhäusler J, Denk M, Renken F, Kellner L, Schubnell J, et al. Statistical characterization of stress concentrations along butt joint weld seams using deep neural networks. Appl Sci 2022;12(6089):1–17. https://doi.org/10.3390/app12126089.
[32] Teng T-L, Fung C-P, Chang P-H. Effect of weld geometry and residual stresses on fatigue in butt-welded joints. Int J Press Vessel Pip 2002;79:467–82. https://doi.org/10.1016/S0308-0161(02)00060-1.
[33] Gao H, Zhang X, Huang P, Jiang H, Li Z. Fatigue reliability of welded joints accounting for uncertainties in weld geometry. Adv Mech Eng 2022;14:1–9. https://doi.org/10.1177/16878132221098892.
[34] Cerit M, Kokumer O, Genel K. Stress concentration effects of undercut defect and reinforcement metal in butt welded joint. Eng Fail Anal 2010;17:571–8. https://doi.org/10.1016/j.engfailanal.2009.10.010.
[35] Niraula A, Remes H, Lehto P. Local weld geometry - based characterization of fatigue strength in laser - MAG hybrid welded joints. Weld World 2023;67:1527–44. https://doi.org/10.1007/s40194-023-01488-5.
[36] Bell R, Vosikovsky O, Bain SA. The significance of weld toe undercuts in the fatigue of steel plate T-joints. Int J Fatigue 1989;11:3–11. https://doi.org/10.1016/0142-1123(89)90041-8.
[37] Wang T, Yang JG, Liu XS, Dong ZB, Fang HY. Stress intensity factor expression for center-cracked butt joint considering the effect of joint shape. Mater Des 2012;35:72–9. https://doi.org/10.1016/j.matdes.2011.09.020.
[38] Laguna EH, De La Peña NA, De Los Ríos OA. Fracture mechanics assessment of fatigue semi-elliptical cracks in butt-welded joints. Ingeniare 2018;26:568–76. https://doi.org/10.4067/S0718-33052018000400568.
[39] Schork B, Zerbst U, Kiyak Y, Kaffenberger M, Madia M, Oechsner M. Effect of the parameters of weld toe geometry on the FAT class as obtained by means of fracture mechanics-based simulations. Weld World 2020;64:925–36. https://doi.org/10.1007/s40194-020-00874-7.
[40] Schubnell J, Jung M, Le CH, Farajian M, Braun M, Ehlers S, et al. Influence of the optical measurement technique and evaluation approach on the determination of local weld geometry parameters for different weld types. Weld World 2020;64:301–16. https://doi.org/10.1177/0954405412439138.
[41] Walfish S. A review of statistical outlier methods. Pharm Technol 2006;30:82–6.
[42] Ho NJ. The fatigue of weldments subjected to complex loading. University of Illinois 1984.
[43] Kiyak Y, Madia M, Zerbst U. Extended parametric equations for weld toe stress concentration factors and through-thickness stress distributions in butt-welded plates subject to tensile and bending loading. Weld World 2016;60:1247–59. https://doi.org/10.1007/s40194-016-0377-x.